*Article*

# Analytical Solution for Impact of Caputo-Fabrizio Fractional Derivative on MHD Casson Fluid with Thermal Radiation and Chemical Reaction Effects

**Ridhwan Reyaz** [†] **, Ahmad Qushairi Mohamad** *,[†] **, Yeou Jiann Lim** [†] **, Muhammad Saqib** **and Sharidan Shafie**

Department of Mathematical Sciences, Faculty of Science, Universiti Teknologi Malaysia, Johor Bahru 81310, Malaysia; mridhwan45@graduate.utm.my (R.R.); jiann@utm.my (Y.J.L.); saqib@graduate.utm.my (M.S.); sharidan@utm.my (S.S.)

* Correspondence: ahmadqushairi@utm.my; Tel.: +60-13-767-8687

† These authors contributed equally to this work.

**Abstract:** Fractional derivatives have been proven to showcase a spectrum of solutions that is useful in the fields of engineering, medical, and manufacturing sciences. Studies on the application of fractional derivatives on fluid flow are relatively new, especially in analytical studies. Thus, geometrical representations for fractional derivatives in the mechanics of fluid flows are yet to be discovered. Nonetheless, theoretical studies will be useful in facilitating future experimental studies. Therefore, the aim of this study is to showcase an analytical solution on the impact of the Caputo-Fabrizio fractional derivative for a magnethohydrodynamic (MHD) Casson fluid flow with thermal radiation and chemical reaction. Analytical solutions are obtained via Laplace transform through compound functions. The obtained solutions are first verified, then analysed. It is observed from the study that variations in the fractional derivative parameter, $\alpha$, exhibits a transitional behaviour of fluid between unsteady state and steady state. Numerical analyses on skin friction, Nusselt number, and Sherwood number were also analysed. Behaviour of these three properties were in agreement of that from past literature.

**Keywords:** laplace transform; Caputo-Fabrizio fractional derivative; Casson fluid; thermal radiation; chemical reaction

## 1. Introduction

Non-Newtonian fluids have been recognised as one of the most popular research topics not only in the field of fluid mechanics but also in production engineering, chemical engineering, as well as the manufacturing process. Behaviour of non-Newtonian fluid varies according to its subclass category and the amount of shear stress applied on it. For instance, ketchup would flow easily when shaken harder or corn starch would solidify when slapped at full speed. These characteristics are what classify as a non-Newtonian fluid. Due to the complexity of non-Newtonian fluids, the traditional constitutive equations are unable to express the fluid adequately. No single equation as of today could describe a non-Newtonian fluid comprehensively. As such, several models have been developed over the years to investigate the properties of these fluids such as the Maxwell fluid, Oldroyd-B fluid, Walters'-B fluid, second grade fluid, and third grade fluid [1]. For instance, Baranovskii and Artemov [2] did a study by proving the existence of global weak solutions on the system of partial differential equations for an unsteady flow of Oldroyd fluid. One of the most popular non-Newtonian fluids is the Casson fluid. A Casson fluid behaves such that it will act solid when sheer stress applied is less than its yield stress. However, when sheer stress applied is more that its yield stress the fluid will be in motion [3]. The Casson fluid model was first introduced by Casson [4] in 1959 whilst investigating the rheological data of pigment ink in a printer. Examples of recent research on Casson fluids can be found

in [5,6]. Over the past few decades, research on Casson fluids have increased drastically. Frigaard [7] did an extensive review on non-Newtonian fluids, including Casson fluids, comparing and analysing their behaviour with variations of sheer stress applied to various fluids with different yield stress. Meanwhile, Gbadeyan [8] reviewed various physical effects on Casson fluids. Effects concerned include magnethohydrodynamic (MHD) and thermal radiation effects.

Hussanan et al. [9], investigated the behaviour of a Casson fluid over an oscillating plate with the presence of Newtonian heating. From the study, it is concluded that as the Casson parameter increases, the fluid velocity decreases. Increasing the Newtonian heating parameter would also increase the fluid velocity. The study only considered a normal oscillating plate and not an accelerated plate as well as the presence of Newtonian heating. In another study, Hussanan et al. [10] extended the same problem by considering the MHD effect. Khalid et al. [11] did a similar study as Hussanan et al. [9], by considering the effect of a constant wall temperature instead of Newtonian heating. Findings of Khalid et al. [11] were aligned with Hussanan et al. [9]. Khalid et al. [12] then extended their study of Casson fluids by considering the effect of porous medium with similar boundary conditions. The authors of the study found that as the porosity parameter increases, fluid velocity is also increased. Kataria and Patel [13] on the other hand, examined a Casson fluid flow with effects of MHD, thermal radiation, and chemical reaction through a porous medium. The thermal radiation effect in this study is considered to be linear. This is observed in the governing equation where the derivative of $T$ with respect to $x$ is of order one. A non-linear thermal radiation effect would have a second-order $T$ derivative. Mixed convection flow, isothermal, and ramped wall temperature over a vertical oscillating plate were also considered in the study of Kataria and Patel [13]. The temperature of the fluid would vary according to time, $t$, due to the characteristics of boundary conditions applied.

Recently, Khan et al. [14] replicated Kataria and Patel [13] by considering a special case of an accelerated plate from solutions with an oscillating plate and replacing the thermal radiation effect with Newtonian heating. Later on, Kataria and Patel [15] revisited the previous study and considered not just ramped temperature but a ramped concentration as well. Instead of thermal radiation, the authors also considered heat absorption or generation effect on an exponentially accelerated plate. Naqvi et al. [16] examined a Casson fluid flow over a porous stretching cylinder with the presence of nanoparticles in the fluid. Meanwhile, Rao et al. [17] conducted a study to investigate the behaviour of a Casson fluid with the presence of a MHD effect, radiation absorption, as well as heat generation or absorption.

Studies of non-Newtonian fluid flow mentioned previously did not consider the application of fractional derivatives. The study of fractional derivatives on a non-Newtonian fluid flow was first instigated by Khan et al. [18]. They investigated fractional Casson fluid flow by introducing the Caputo fractional derivative into the governing equation. Fractional derivatives are simply defined as derivatives with order between zero and one. This was first mentioned by L'Hospital when he wrote a letter to Leibniez [19] asking what would happen if the $n$ notation of a derivative would be a fraction, complex, or an arbitrary number. Since then, many researchers have attempted to define a fractional derivative, including Riemann, Abel, and Liouville [20]. The Riemann–Liouville, Grunwald–Letnikov, and Caputo derivates are a few of the most popular definitions used to date [21,22]. One of the latest definition of a fractional derivative were introduced by Atangana and Baleanu [23] back in 2016. The new definition that does not have a non-local and non-singular kernel is now known as the Atangana–Baleanu (AB) fractional derivative. Research on fractional derivatives has increased over the past few decades. Fractional derivatives have been applied in many fields including mechanical engineering, civil engineering, and numerical analysis. For example, Cao et al. [24] used Riemann–Liouville fractional derivative to calculate the shear stress of a beam by performing Laplace transform on the fractional Euler–Lagrange equation. Meanwhile, Gomez et al. [25] applied not only the Riemann–Liouville, as well as the Grunwald–Letnikov, Liouville–Caputo, and Caputo-Fabrizio fractional derivative to model electrical circuits. Atangana and Baleanu

presented a study on the impact of the Caputo-Fabrizio fractional derivative on groundwater flow within a confined aquifer [26]. Analytical solutions of the groundwater flow model were presented and compared with experimental data. Results presented suggest that the obtained analytical solutions are in good agreement with experimental data. Other than that, the authors also presented another study on the applications of the Caputo–Liouville derivative on the fixed point theorem for nonlinear Schrodinger equation stability analysis [27]. On the other hand, Yuan and Zhang [28] conducted an investigation on the fractional Laplacian Oldroyd-B model for global well-posedness solutions. Lastly, Saad et al. presented two studies on the applications of the new AB derivative. The authors used fractional derivatives on the Burgers, the Korteweg–de Vries, and the Korteweg–de Vries–Burgers equations [29,30]. In theoretical turbulence research, nonlocal and fractional derivatives are presently introduced to describe Reynolds shear stresses [31] and to improve Large Eddy Simulation (LES) applications [32,33].

Meanwhile, discussing fractional derivatives applied in boundary layer flow problems, Atangana and Baleanu [34] investigated the impact of fractional derivatives on a parabolic differential equation. The parabolic equation was first incorporated with the Caputo derivative and then solved, both explicitly and implicitly, via the finite difference method. The authors later on presented another study on the application of the new AB derivative on a heat transfer model back in 2016 [23]. On the other hand, Ali et al. [35] extended the work done by Khan et al. [18] by considering an oscillating plate. Ali et al. [35] however, only considered cosine oscillations of the plate and did not consider the sine oscillation. Khan et al. [36] took another approach in another study and investigated a fractional Casson fluid using a semi-analytical approach where analytical solutions in the time domain were not presented in the study. The boundary value problem was solved using Laplace transform to obtain solutions in the frequency domain, and inverse Laplace transform via the Zakian method, presenting their final solutions of numerical solutions. The exact inverse solutions were not determined possibly due to the complexity of the problem, as fluid flow within a micro-channel with fractional derivatives was considered. Other than that, Sheikh et al. [37] presented a comparative study on the Caputo-Fabrizio (CF) and the Atangana–Baleanu (AB) fractional derivatives for a mixed convection flow of a Casson fluid. This problem was solved analytically using the Laplace transform, but solutions were presented with special functions such as the Wright function and the Mittag–Lefler function. From the study, the authors concluded that there exist a slight difference between solutions of CF- and AB-type fractional derivatives in the velocity profile. The difference in the velocity profile will increase as $t \rightarrow \infty$. Sheikh et al. [38] extended their study by considering the effects of a chemical reaction, heat absorption, and generation. The new study produced the same result as the last one, thus concretizing the outcome on the behaviour of fluid with different fractional definitions. Maiti et al. [6] studied the heat and mass transfer of a Casson fluid with effects of an MHD and thermal radiation through a porous cylindrical tube. The governing equations were modified using the Caputo-Fabrizio fractional derivative. The authors aimed to examine heat and mass transfer through an arterial segment whilst there is a magnetic field and thermal radiation present in an accelerated body. The final solution was obtained analytically using Laplace and Hankel transforms.

Although numerous studies on the application of fractional derivatives on non-Newtonian fluid have been done, the geometrical representations of the fractional parameter has yet to be discovered. Nonetheless, as shown by the study of Atangana and Baleanu [26], solutions provided by these studies could be useful for validating future experimental studies. Past studies lack in providing clear analytical solutions without any special functions such as the Wright function and the Mittag–Lefler function as they contained various singularities. Therefore, motivated by this, the current study aims to produce analytical solutions using the Caputo-Fabrizio fractional derivatives, without any special functions, for the velocity, temperature, and concentration profiles for a free convection flow of a Casson fluid over an accelerated plate with an MHD, non-linear thermal radiation, chemical reaction, and porous medium effects. To the authors' best

knowledge, an up-to-present study on analytical solutions for heat and mass transfer of fractional Caputo-Fabrizio MHD Casson fluid over an accelerated plate through porous medium with effects of thermal radiation and chemical reaction has not been conducted in the literature.

## 2. Problem Formulation

Heat and mass transfer of a Casson fluid flow with effects of magnetic field, non-linear thermal radiation, and chemical reaction in a porous medium over an accelerated plate is considered. At $t = 0$, the plate and fluid are both at rest with constant temperature and concentration, $T_\infty$ and $C_\infty$, respectively. When $t \geq 0$, the temperature and concentration of the plate are increased to $T_W$ as well as $C_W$, respectively, and remain constant thereafter. At $t \geq 0$, the plate begins to increase its speed uniformly at the rate of, $At$, where $A$ is the acceleration. A permeated uniform magnetic field, $B_0$, parallel to the $y$-axis is applied to the fluid. Non-linear thermal radiation, $q_r$, is applied perpendicular to the $x$-axis. Due to the small Reynold number, effects of an induced magnetic field in the fluid flow is insignificant enough for it to be neglected. The $y$ coordinate, pointing perpendicular to the plate, constricts fluid flow at $y > 0$. The velocity, $U$, temperature, $T$, and concentration, $C$, are all dependent on space variable, $y$, and time, $t$. Figure 1 illustrates the physical representation of the fluid flow.
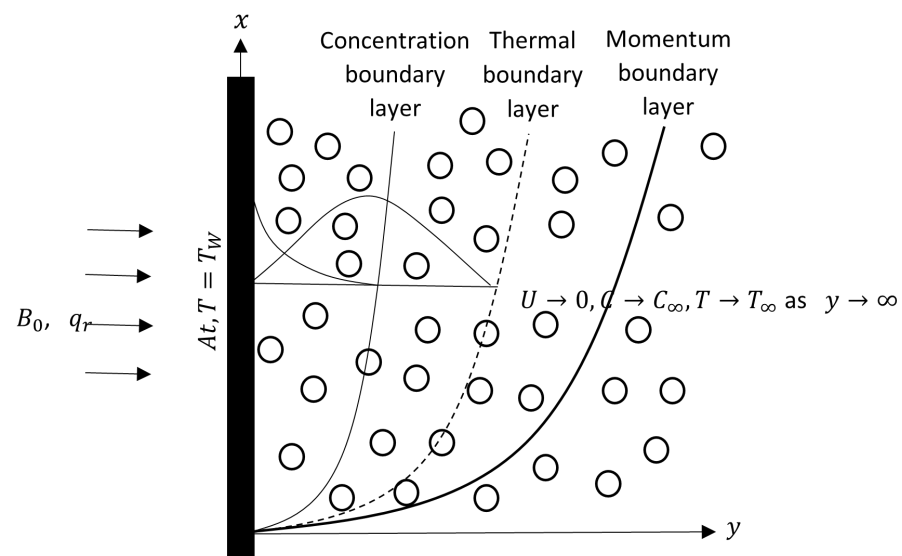


**Figure 1.** Physical configuration.

With considerations mentioned above and bearing in mind Boussinesq's approximation, the governing equations for the Casson fluid flow are obtained as follows [6,39,40]:

$$\rho \frac{\partial U(y,t)}{\partial t} = \mu \left(1 + \frac{1}{\beta}\right) \frac{\partial^2 U(y,t)}{\partial y^2} - \left(\sigma B_0^2 + \frac{\mu}{k}\right) U(y,t)$$

$$+ \rho g \beta_T (T - T_\infty) + \rho g \beta_C (C - C_\infty), \tag{1}$$

$$\rho C_p \frac{\partial T(y,t)}{\partial t} = k_1 \frac{\partial^2 T(y,t)}{\partial y^2} - \frac{\partial q_r}{\partial y}, \tag{2}$$

$$\frac{\partial C(y,t)}{\partial t} = D \frac{\partial^2 C(y,t)}{\partial y^2} - k_2 (C - C_\infty), \tag{3}$$

together with its initial and boundary conditions:

$$U(y,0) = 0, \quad T(y,0) = T_\infty, \quad C(y,0) = C_\infty,$$
$$U(0,t) = At, \quad T(0,t) = T_W, \quad C(0,t) = C_W, \tag{4}$$
$$U(\infty,t) = 0, \quad T(\infty,t) = T_\infty, \quad C(\infty,t) = C_\infty.$$

whereby $\rho$ is the density of the fluid, $\mu$ is the viscosity of the fluid, $\beta$ is the Casson parameter, $g$ is the gravitational force, $\beta_T$ is the volumetric thermal coefficient of expansion, $\beta_C$ is the volumetric solutal coefficient of expansion, $\sigma$ is the electrical conductivity, $C_P$ is the specific heat at constant pressure, and $D$ is the mass diffusion coefficient. Here, $k, k_1$, and $k_2$ are the porosity parameter, thermal conductivity parameter, and chemical reaction parameter, respectively.

Incorporating Rosseland's approximation for thermal radiation, the term $q_r$ may be written as follows [41,42]:

$$q_r = -\frac{4\sigma^*}{3k^*}\frac{\partial T^4}{\partial y}, \tag{5}$$

whereby $\sigma^*$ is the Stefan–Boltzman constant, $k^*$ is the mean absorption coefficient, and $T^4$ is the difference in temperature of fluid flow. $T^4$ can be expanded about $T_\infty$ by using a Taylor series and neglecting higher order derivatives as the values are insignificantly small and taking the form of such that $T^4 \equiv 4T_\infty^3 T - 3T_\infty^4$ [1].

Thus, by taking into account Equation (5) and the non-dimensional parameter below, leads to:

$$U^* = \frac{U}{(vA)^{1/3}}, \quad y^* = \frac{yA^{1/3}}{v^{2/3}}, \quad C^* = \frac{C - C_\infty}{C_W - C_\infty},$$
$$\tag{6}$$
$$t^* = \frac{tA^{2/3}}{v^{1/3}}, \quad T^* = \frac{T - T_\infty}{T_W - T_\infty},$$

and dropping the asterisk notation, the dimensionless form of Equations (1)–(4) are written as follows:

$$\frac{\partial U(y,t)}{\partial t} = \frac{1}{\beta_0}\frac{\partial^2 U(y,t)}{\partial y^2} - \left(M^2 + \frac{1}{k'}\right)U(y,t) + GrT(y,t) + GmC(y,t), \tag{7}$$

$$\frac{\partial T(y,t)}{\partial t} = \left(1 + \frac{4}{3}N\right)\frac{1}{Pr}\frac{\partial^2 T(y,t)}{\partial y^2}, \tag{8}$$

$$\frac{\partial C(y,t)}{\partial t} = \frac{1}{Sc}\frac{\partial^2 C(y,t)}{\partial y^2} - RC(y,t), \tag{9}$$

with conditions:

$$U(y,0) = 0, \quad T(y,0) = 0, \quad C(y,0) = 0,$$
$$U(0,t) = t, \quad T(0,t) = 1, \quad C(0,t) = 1, \tag{10}$$
$$U(\infty,t) = 0, \quad T(\infty,t) = 0, \quad C(\infty,t) = 0,$$

where:

$$\beta_0 = \frac{\beta}{\beta+1}, \quad Gr = \frac{g\beta_T(T_W - T_\infty)}{A}, \quad Sc = \frac{v}{D},$$
$$M^2 = \frac{\sigma B_0^2 v^{1/3}}{\rho A^{2/3}}, \quad Gm = \frac{g\beta_C(C_W - C_\infty)}{A}, \quad R = k_2\frac{v^{1/3}}{A^{2/3}}, \tag{11}$$
$$k' = \frac{kA^{2/3}}{v^{4/3}}, \quad N = \frac{4\sigma^* T_\infty^3}{k^* k_1}, \quad Pr = \frac{\mu C_P}{k_1} = \frac{v\rho C_P}{k_1}.$$

Here, $\beta_0$ is the dimensionless Casson parameter, $Gr$ is thermal Grashof number, $Sc$ is Schimdt number, $M$ is the magnetic parameter, $Gm$ is the mass Grashof number, $R$ is the chemical reaction parameter, $k'$ is the permeability parameter, $N$ is the thermal radiation parameter, and $Pr$ is the Prandtl number.

Then, the Caputo-Fabrizio fractional derivative is utilised within the classical derivatives with respect to time, by replacing the $\frac{\delta}{\delta t}(\cdot)$ with $D_t^\alpha(\cdot)$, from Equations (7)–(9). Thus, converting the equations to a fractional model such as [43,44]:

$$D_t^\alpha U(y,t) = \frac{1}{\beta_0}\frac{\partial^2 U(y,t)}{\partial y^2} - \left(M^2 + \frac{1}{k'}\right)U(y,t) + GrT(y,t) + GmC(y,t), \tag{12}$$

$$D_t^\alpha T(y,t) = \left(1 + \frac{4}{3}N\right)\frac{1}{Pr}\frac{\partial^2 T(y,t)}{\partial y^2}, \tag{13}$$

$$D_t^\alpha C(y,t) = \frac{1}{Sc}\frac{\partial^2 C(y,t)}{\partial y^2} - RC(y,t), \tag{14}$$

where:

$$D_t^\alpha f(x,t) = \frac{1}{1-\alpha}\int_0^t \frac{\partial f(x,s)}{\partial x}exp\left(-\alpha\frac{t-s}{1-\alpha}\right)ds, \tag{15}$$

is the singular kernel Caputo-Fabrizio fractional derivative. Its Laplace transform can be written as [44,45]:

$$\mathcal{L}\{D_t^\alpha f(x,t)\} = \frac{q\bar{f}(x,q) - f(x,0)}{q + \alpha(1-q)}, \tag{16}$$

where $\alpha$ is the fractional derivative parameter.

## 3. Solutions to the Problem

Solutions to this problem are calculated analytically by using the Laplace transform. From a partial derivative system of equations, it is reduced to an ordinary derivative system of equations. Method of undetermined coefficient is then used to solve the system of ODE. The final solutions are obtained via the inverse Laplace transform.

By using Equation (16) and some basic Laplace transform, subjected to conditions (10), the solutions of Equations (12)–(14) in terms of Laplace variables can be written as:

$$\bar{U}(y,q) = \left[\frac{1}{q^2} + \frac{Gr_0}{q}\left(\frac{q+a_1}{a_6q-a_5}\right) + \frac{Gm_0}{q}\left(\frac{q+a_1}{a_7q+a_8}\right)\right]\exp\left(-y\sqrt{\frac{a_4q+a_5}{q+a_1}}\right)$$

$$-\frac{Gr_0}{q}\left(\frac{q+a_1}{a_6q-a_5}\right)\exp\left(-y\sqrt{\frac{Pr_0 a_0 q}{q+a_1}}\right) \tag{17}$$

$$-\frac{Gm_0}{q}\left(\frac{q+a_1}{a_7q+a_8}\right)\exp\left(-y\sqrt{\frac{a_2q+a_3}{q+a_1}}\right),$$

$$\bar{T}(y,q) = \frac{1}{q}\exp\left(-y\sqrt{\frac{Pr_0 a_0 q}{q+a_1}}\right), \tag{18}$$

$$\bar{C}(y,q) = \frac{1}{q}\exp\left(-y\sqrt{\frac{a_2q+a_3}{q+a_1}}\right), \tag{19}$$

where:

$$a_0 = \frac{1}{1-\alpha}, \qquad a_3 = Sca_1 R, \qquad a_6 = Pr_0 a_0 - a_4,$$

$$a_1 = \alpha a_0, \qquad a_4 = M_0 + k_0' + a_0 \beta_0, \quad a_7 = a_2 - a_4,$$

$$a_2 = Sc(a_0 + R), \quad a_5 = a_1 M_0 + a_1 k_0', \qquad a_8 = a_3 - a_5,$$

$$M_0 = \beta_0 M^2, \qquad Gr_0 = Gr\beta_0, \qquad Gm_0 = Gm\beta_0,$$

$$Pr_0 = \frac{Pr}{1 + \frac{4}{3}N}, \qquad k_0' = \frac{\beta_0}{k'}.$$

are constant parameters. An inverse Laplace transform of Equations (17)–(19) is then calculated to obtain the analytical solutions. Final analytical solutions of velocity, temperature, and concentration profiles are determined as:

$$U(y,t) = A_1(y,t) + A_2(y,t) + A_3(y,t) + A_4(y,t) + A_5(y,t), \tag{20}$$

$$T(y,t) = B_1(y,t), \tag{21}$$

$$C(y,t) = C_1(y,t), \tag{22}$$

where:

$$
\begin{aligned}
A_1(y,t) = & \int_0^\infty \frac{\sqrt{a_4}}{2\sqrt{\pi}u^{3/2}} \exp\left(\frac{-a_4}{4u} - uy^2\right)(t)[2\Phi(t) - 1]du \\
& + \int_0^\infty \int_0^t \int_0^\pi \frac{-1}{\pi} \frac{\sqrt{a_4}}{2\sqrt{\pi}u^{3/2}} \frac{\sqrt{a_{12}uy^2}}{\sqrt{s}}(t-s) \\
& \cos\left[\tau - \left(2\sqrt{a_{12}uy^2 s}\right)\sin(\tau)\right] \\
& \exp\left(\frac{-a_4}{4u} - uy^2 - a_1 s\right)d\tau ds du,
\end{aligned}
\tag{23}
$$

$$
\begin{aligned}
A_2(y,t) = & \int_0^\infty a_{14} Gr_0 \frac{-\sqrt{a_4}}{2\sqrt{\pi}u^{3/2}} \exp\left(\frac{-a_4}{4u} - uy^2\right)[2\Phi(t) - 1]du \\
& + \int_0^\infty a_{13} Gr_0 \frac{\sqrt{a_4}}{2\sqrt{\pi}u^{3/2}} \exp\left(\frac{-a_4}{4u} - uy^2 + \frac{a_5 t}{a_6}\right) \\
& [2\Phi(t) - 1]du \\
& + \int_0^\infty \int_0^t \int_0^\pi \frac{-1}{\pi}\left[a_{13} Gr_0 \exp\left(\frac{a_5(t-s)}{a_6}\right) - a_{14} Gr_0\right] \\
& \frac{\sqrt{a_4}}{2\sqrt{\pi}u^{3/2}} \frac{\sqrt{a_{12}uy^2}}{\sqrt{s}} \cos\left[\tau - \left(2\sqrt{a_{12}uy^2 s}\right)\sin(\tau)\right] \\
& \exp\left(\frac{-a_4}{4u} - uy^2 - a_1 s\right)d\tau ds du,
\end{aligned}
\tag{24}
$$

$$
\begin{aligned}
A_3(y,t) = \quad & \int_0^\infty a_{15} G m_0 \frac{\sqrt{a_4}}{2\sqrt{\pi} u^{3/2}} \exp\left(\frac{-a_4}{4u} - uy^2\right) [2\Phi(t) - 1] du \\
& + \int_0^\infty a_{16} G m_0 \frac{\sqrt{a_4}}{2\sqrt{\pi} u^{3/2}} \exp\left(\frac{-a_4}{4u} - uy^2 - \frac{a_8 t}{a_7}\right) \\
& [2\Phi(t) - 1] du \\
& + \int_0^\infty \int_0^t \int_0^\pi \frac{-1}{\pi} \left[ a_{16} G m_0 \exp\left(\frac{-a_8(t-s)}{a_7}\right) + a_{15} G m_0 \right] \\
& \frac{\sqrt{a_4}}{2\sqrt{\pi} u^{3/2}} \frac{\sqrt{a_{12} u y^2}}{\sqrt{s}} \cos\left[\tau - \left(2\sqrt{a_{12} u y^2 s}\right) \sin(\tau)\right] \\
& \exp\left(\frac{-a_4}{4u} - uy^2 - a_1 s\right) d\tau \, ds \, du,
\end{aligned}
\tag{25}
$$

$$
\begin{aligned}
A_4(y,t) = \quad & \int_0^\infty a_{14} G r_0 \frac{\sqrt{a_0 P r_0}}{2\sqrt{\pi} u^{3/2}} \exp\left(\frac{-a_0 P r_0}{4u} - uy^2\right) [2\Phi(t) - 1] du \\
& + \int_0^\infty -a_{13} G r_0 \frac{\sqrt{a_0 P r_0}}{2\sqrt{\pi} u^{3/2}} \exp\left(\frac{-a_0 P r_0}{4u} - uy^2 + \frac{a_5 t}{a_6}\right) \\
& [2\Phi(t) - 1] du \\
& + \int_0^\infty \int_0^t \int_0^\pi \frac{1}{\pi} \left[ -a_{13} G r_0 \exp\left(\frac{a_5(t-s)}{a_6}\right) + a_{14} G r_0 \right] \\
& \frac{\sqrt{a_0 P r_0}}{2\sqrt{\pi} u^{3/2}} \frac{\sqrt{a_1 u y^2}}{\sqrt{s}} \cos(\theta) \exp\left[\left(2\sqrt{a_1 u y^2 s}\right) \cos(\theta)\right] \\
& \exp\left(\frac{-a_0 P r_0}{4u} - uy^2 - a_1 s\right) d\theta \, ds \, du,
\end{aligned}
\tag{26}
$$

$$
\begin{aligned}
A_5(y,t) = \quad & \int_0^\infty -a_{15} G m_0 \frac{\sqrt{a_2}}{2\sqrt{\pi} u^{3/2}} \exp\left(\frac{-a_2}{4u} - uy^2\right) [2\Phi(t) - 1] du \\
& + \int_0^\infty -a_{16} G m_0 \frac{\sqrt{a_2}}{2\sqrt{\pi} u^{3/2}} \exp\left(\frac{-a_2}{4u} - uy^2 - \frac{a_8 t}{a_7}\right) \\
& [2\Phi(t) - 1] du \\
& + \int_0^\infty \int_0^t \int_0^\pi \frac{1}{\pi} \left[ a_{16} G m_0 \exp\left(\frac{-a_8(t-s)}{a_7}\right) + a_{15} G m_0 \right] \\
& \frac{\sqrt{a_2}}{2\sqrt{\pi} u^{3/2}} \frac{\sqrt{a_{10} u y^2}}{\sqrt{s}} \cos\left[\tau - \left(2\sqrt{a_{10} u y^2 s}\right) \sin(\tau)\right] \\
& \exp\left(\frac{-a_2}{4u} - uy^2 - a_1 s\right) d\tau \, ds \, du,
\end{aligned}
\tag{27}
$$

$$B_1(y,t) = \int_0^\infty \frac{\sqrt{a_0 Pr_0}}{2\sqrt{\pi}u^{3/2}} \exp\left(\frac{-a_0 Pr_0}{4u} - uy^2\right)[2\Phi(t) - 1]du$$

$$+ \int_0^\infty \int_0^t \int_0^\pi \frac{1}{\pi} \frac{\sqrt{a_0 Pr_0}}{2\sqrt{\pi}u^{3/2}} \frac{\sqrt{a_1 uy^2}}{\sqrt{s}} \cos(\theta)$$

$$\exp\left[\left(2\sqrt{a_1 uy^2 s}\right)\cos(\theta)\right]$$

$$\exp\left(\frac{-a_0 Pr_0}{4u} - uy^2 - a_1 s\right)d\theta ds du, \tag{28}$$

$$C_1(y,t) = \int_0^\infty \frac{\sqrt{a_2}}{2\sqrt{\pi}u^{3/2}} \exp\left(\frac{-a_2}{4u} - uy^2\right)[2\Phi(t) - 1]du$$

$$+ \int_0^\infty \int_0^t \int_0^\pi \frac{-1}{\pi} \frac{\sqrt{a_2}}{2\sqrt{\pi}u^{3/2}} \frac{\sqrt{a_{10} uy^2}}{\sqrt{s}}$$

$$\cos\left[\tau - \left(2\sqrt{a_{10} uy^2 s}\right)\sin(\tau)\right]$$

$$\exp\left(\frac{-a_2}{4u} - uy^2 - a_1 s\right)d\tau ds du, \tag{29}$$

where:

$$a_9 = \frac{a_3}{a_2}, \qquad a_{12} = a_{11} - a_1, \qquad a_{15} = \frac{a_1}{a_8},$$

$$a_{10} = a_9 - a_1, \quad a_{13} = \frac{a_5 + a_1 a_6}{a_5 a_6}, \quad a_{16} = \frac{(-a_1 a_7 + a_8)}{a_7 a_8},$$

$$a_{11} = \frac{a_5}{a_4}, \qquad a_{14} = \frac{a_1}{a_5},$$

are constant parameters and $\Phi(t)$ is the Heaviside step function.

### 3.1. Non-Fractional Casson Fluid Solution

Fractional parameter of solutions from Equations (20)–(22) are represented by notation $\alpha$. By setting $\alpha = 1$ and using the Laplace inverse transform as well as the shifting theorem, the non-fractional Casson fluid flow solutions are obtained and presented as follows:

$$U_1(y,t) = D_1(y,t) + D_2(y,t) + D_3(y,t) + D_4(y,t) + D_5(y,t), \tag{30}$$

$$T_1(y,t) = F_1(y,t), \tag{31}$$

$$C_1(y,t) = G_1(y,t), \tag{32}$$

where:

$$D_1(y,t) = \frac{1}{4\sqrt{b_1}} \exp\left(-y\sqrt{b_1}\right)\left[\left(2t\sqrt{b_1} - \beta_0 y\right)\left(1 + \mathrm{erf}\left(\frac{2t\sqrt{b_1} - \beta_0 y}{2\sqrt{\beta_0 t}}\right)\right)\right.$$

$$\left. \exp\left(2y\sqrt{b_1}\right)\left(2t\sqrt{b_1} + \beta_0 y\right)\mathrm{erfc}\left(\frac{2t\sqrt{b_1} + \beta_0 y}{2\sqrt{\beta_0 t}}\right)\right], \tag{33}$$

$$
D_2(y,t) = \frac{Gr_0}{2b_1}\left[\exp\left(-y\sqrt{b_1}\right)\left(-1 + \mathrm{erfc}\left(\frac{2t\sqrt{b_1} - \beta_0 y}{2\sqrt{\beta_0 t}}\right)\right.\right.
$$

$$
\left.- \exp\left(-y\sqrt{b_1}\right)\mathrm{erfc}\left(\frac{2t\sqrt{b_1} + \beta_0 y}{2\sqrt{\beta_0 t}}\right)\right)
$$

$$
\exp\left(\frac{b_1 t}{b_2} - y\sqrt{\frac{b_1}{b_2}(\beta_0 + b_2)}\right)
$$

$$
\left(2 - \mathrm{erfc}\left(\frac{2t\sqrt{\frac{b_1}{b_2}(\beta_0 + b_2)} - \beta_0 y}{2\sqrt{\beta_0 t}}\right)\right)
$$

$$
+ \exp\left(2y\sqrt{\frac{b_1}{b_2}(\beta_0 + b_2)}\right)
$$

$$
\left.\mathrm{erfc}\left(\frac{2t\sqrt{\frac{b_1}{b_2}(\beta_0 + b_2)} + \beta_0 y}{2\sqrt{\beta_0 t}}\right)\right)\right],
$$

(34)

$$
D_3(y,t) = \frac{Gm_0}{2b_4}\left[\exp\left(-y\sqrt{b_1}\right)\left(-1 + \mathrm{erfc}\left(\frac{2t\sqrt{b_1} - \beta_0 y}{2\sqrt{\beta_0 t}}\right)\right.\right.
$$

$$
\left.- \exp\left(-y\sqrt{b_1}\right)\mathrm{erfc}\left(\frac{2t\sqrt{b_1} + \beta_0 y}{2\sqrt{\beta_0 t}}\right)\right)
$$

$$
\exp\left(\frac{b_4 t}{b_3} - y\sqrt{b_1 + \frac{\beta_0 b_4}{b_3}}\right)
$$

$$
\left(2 - \mathrm{erfc}\left(\frac{2t\sqrt{b_1 + \frac{\beta_0 b_4}{b_3}} - \beta_0 y}{2\sqrt{\beta_0 t}}\right)\right)
$$

$$
+ \exp\left(2y\sqrt{b_1 + \frac{\beta_0 b_4}{b_3}}\right)
$$

$$
\left.\mathrm{erfc}\left(\frac{2t\sqrt{b_1 + \frac{\beta_0 b_4}{b_3}} + \beta_0 y}{2\sqrt{\beta_0 t}}\right)\right)\right],
$$

(35)

$$
D_4(y,t) = -\frac{Gr_0}{2b_1}\left[-2\,\mathrm{erfc}\,\frac{y\sqrt{Pr_0}}{2\sqrt{t}}\right.
$$

$$
+ \exp\left(\frac{b_1 t}{b_2} - y\sqrt{\frac{b_1 Pr_0}{b_2}}\right)\left(1 + \mathrm{erf}\left(\frac{2t\sqrt{\frac{b_1}{b_2}} - y\sqrt{Pr_0}}{2\sqrt{t}}\right)\right)
$$

$$
\left.+ \exp\left(2y\sqrt{\frac{b_1 Pr_0}{b_2}}\right)\mathrm{erfc}\left(\frac{2t\sqrt{\frac{b_1}{b_2}} + y\sqrt{Pr_0}}{2\sqrt{t}}\right)\right)\right],
$$

(36)

$$D_5(y,t) = -\frac{Gm_0}{2b_4}\left[\exp\left(-y\sqrt{-R_0}\right)\right.$$

$$\left(\left(-2 + \text{erfc}\left(\frac{2t\sqrt{-R_0} - Scy}{2\sqrt{Sct}}\right)\right)\right)$$

$$- \exp\left(2y\sqrt{-R_0}\right)\text{erfc}\left(\frac{2t\sqrt{-R_0} + Scy}{2\sqrt{Sct}}\right)\right)$$

$$+ \exp\left(\frac{b_4 t}{b_3} - y\sqrt{\frac{b_4 Sc}{b_3} - R_0}\right)$$

$$\left(2 - \text{erfc}\left(\frac{2t\sqrt{\frac{b_4 Sc}{b_3} - R_0} - Scy}{2\sqrt{Sct}}\right)\right)$$

$$+ \exp\left(2y\sqrt{\frac{b_4 Sc}{b_3} - R_0}\right)$$

$$\left.\text{erfc}\left(\frac{2t\sqrt{\frac{b_4 Sc}{b_3} - R_0} + Scy}{2\sqrt{Sct}}\right)\right)\right],$$

(37)

$$F_1(y,t) = \text{erfc}\left(\frac{\sqrt{Pr_0}}{2\sqrt{t}}y\right),$$

(38)

$$G_1(y,t) = \frac{1}{2}\exp\left(-y\sqrt{-R_0}\right)\left[2 - \text{erfc}\left(\frac{2t\sqrt{-R_0} - Scy}{2\sqrt{Sct}}\right)\right.$$

$$\left.\exp\left(2y\sqrt{-R_0}\right)\text{erfc}\left(\frac{2t\sqrt{-R_0} + Scy}{2\sqrt{Sct}}\right)\right],$$

(39)

where:

$$b_1 = M_0 + k_0', \quad b_2 = Pr_0 - \beta_0,$$
$$b_3 = Sc - \beta_0, \quad b_4 = R_0 + b_1,$$
$$R_0 = R \cdot Sc.$$

are the constant parameters.

*3.2. Skin Friction, Nusselt Number, and Sherwood Number*

The skin friction, $\gamma$, Nusselt number, $Nu$, and Sherwood number, $Sh$, are determined as:

$$\gamma = -\frac{1}{\beta_0}\frac{\partial U(y,t)}{\partial y}\bigg|_{y=0},$$

(40)

$$Nu = -\frac{\partial T(y,t)}{\partial y}\bigg|_{y=0},$$

(41)

$$Sh = \frac{\partial C(y,t)}{\partial y}\bigg|_{y=0}.$$

(42)

## 4. Results and Discussion

Graphical and numerical results are computed by using Equations (20)–(22) and (40)–(42), respectively, with Mathcad-15. Initially, the solutions were validated by comparing analytical results with semi-analytical results obtained via the Laplace–Zakian method. Figures 2–4 shows the comparison of velocity, temperature, and concentration profiles between the obtained analytical solutions and the semi-analytical solutions. As observed, each of the analytical solutions for each profiles fits perfectly with its corresponding semi-analytical solutions. To further verify the obtained results, a comparison with published limiting case from Ali et al. [35] was done. The comparison is displayed in Figure 5. It is observed that the obtained results are in excellent agreement with that of Ali et al. [35]. Thus, the analytical solutions obtained from this study is accepted and valid.

Analysis of obtained results begins with Figures 6 and 7. These figures shows the temperature profiles for solutions obtained from Equation (21) with variations in $N$ and Pr, respectively. Both of the figures also show variations in fractional parameter, $\alpha$. From Figure 6, it is observed that if the value of $N$ increases so does the temperature profile. Increasing values of $N$ indicates increasing amount of thermal radiation applied to the fluid. As the amount of thermal radiation increases, the amount of heat applied to the system is also increased, thus increasing the temperature of fluid. Meanwhile, from Figure 7, it is observed that the temperature profile decreases as the Pr value increases. The Prandtl number is defined as the ratio between the diffusivity rate of momentum and diffusivity rate of heat. Hence, the increment of Prandtl number increases the momentum diffusivity and decreases the thermal diffusivity. With a decrease in thermal diffusivity, the amount of heat introduced into the fluid is low, thus the fluid temperature decreases with an increase in the Pr value. From both, Figure 6 and 7, it is shown that the fluid temperature increases as $\alpha$ increases. It is indicated from past literature that the geometrical applications of fractional derivatives has yet to be found. Nonetheless, the behaviour of fluid temperature with variation of $\alpha$, presented in Figure 6 and 7, could be used by experimental researchers to validate their results.

Next, Figures 8 and 9 display the concentration profiles obtained from Equation (22) with variations in $R$ and $Sc$, respectively. Both figures show variations in $\alpha$ as well. It is observed from Figure 8 that as $R$ increases, the concentration profile decreases. The chemical reaction rate, $R$, determines the species concentration. In this study, a destructive chemical reaction was considered. This is noted by the negative value of the chemical reaction rate parameter, $k_2$, in Equation (3). A destructive chemical reaction tends to create a large disturbance, affecting the species concentration. The larger the chemical reaction rate, the larger the disturbance. The species concentration decreases, at the same time, decreasing the concentration of the fluid. Meanwhile in Figure 9, it is observed that increasing the $Sc$ value decreases the concentration profile. The Schmidt number, $Sc$, can be described as ratios between the rate of diffusion of momentum or the kinematic viscosity, and the rate of diffusion of the fluid mass. Increasing the $Sc$ value increases the momentum diffusivity and decreases the mass diffusivity. Thus, with a decrease in the mass diffusivity, the amount of mass introduced into the fluid decreases as well. Consequently, decreasing the concentration of fluid. In both Figures 8 and 9, concentration profiles increases as $\alpha$ increases. As mentioned before, this observed behaviour in variation of the fractional parameter, $\alpha$, could be used in experimental research in the future as a means of validating their results.
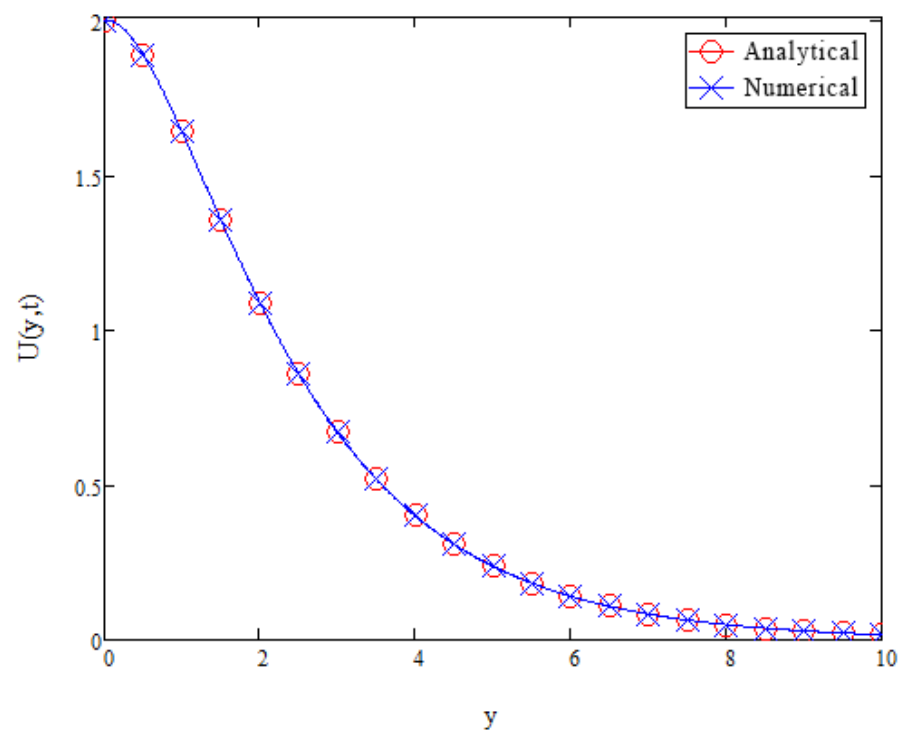
**Figure 2.** Velocity profile for analytical solution presented in Equation (20) validated with numerical solution using Zakian's method.
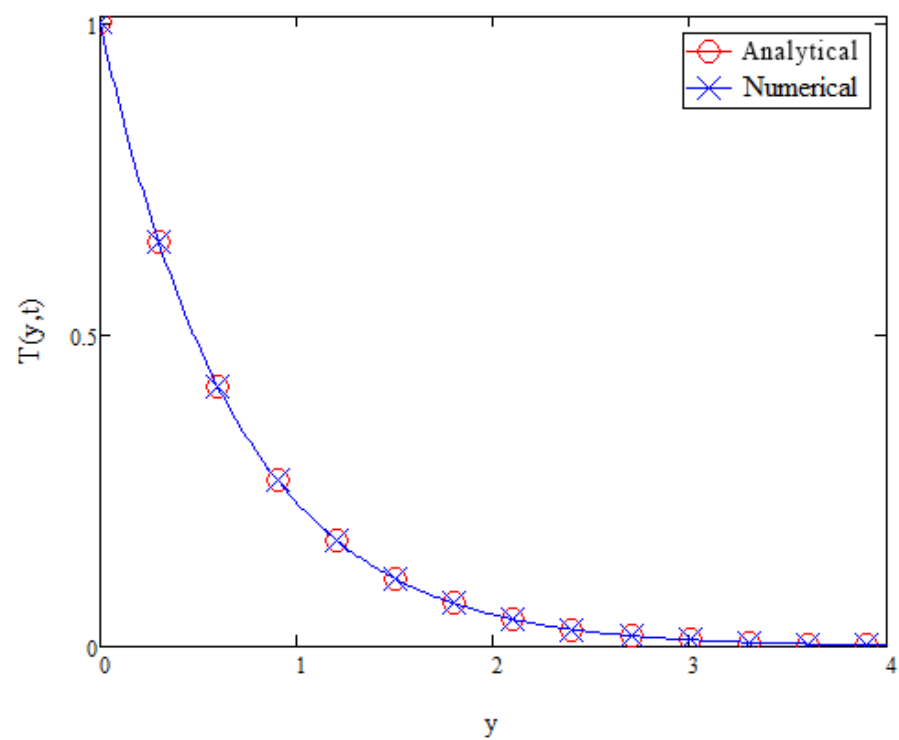


**Figure 3.** Temperature profile for analytical solution presented in Equation (21) validated with numerical solution using Zakian's method.
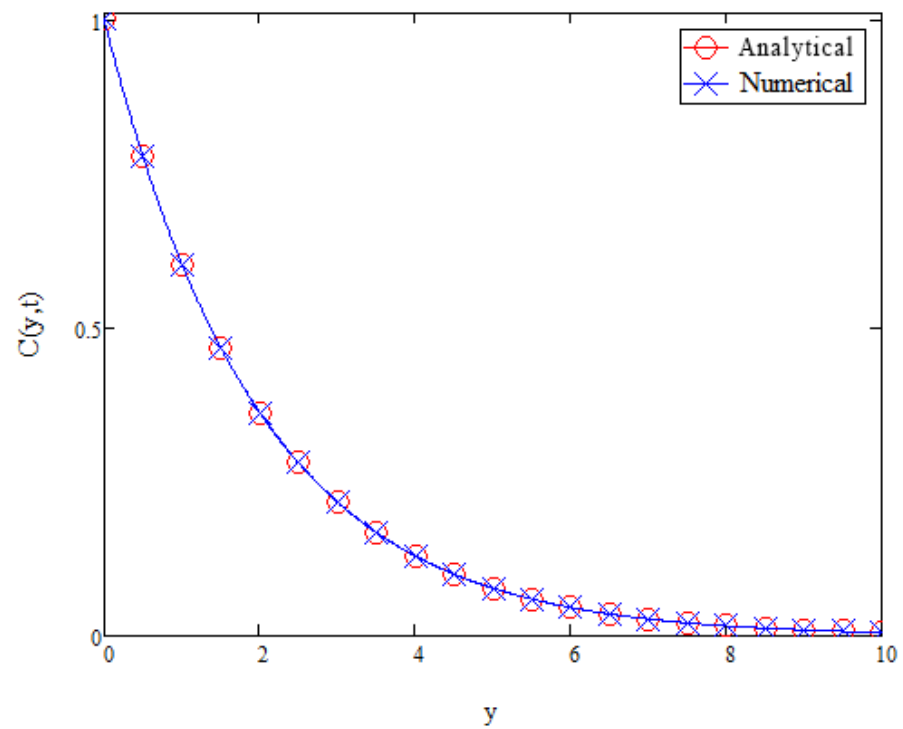
**Figure 4.** Concentration profile for analytical solution presented in Equation (22) validated with numerical solution using Zakian's method.
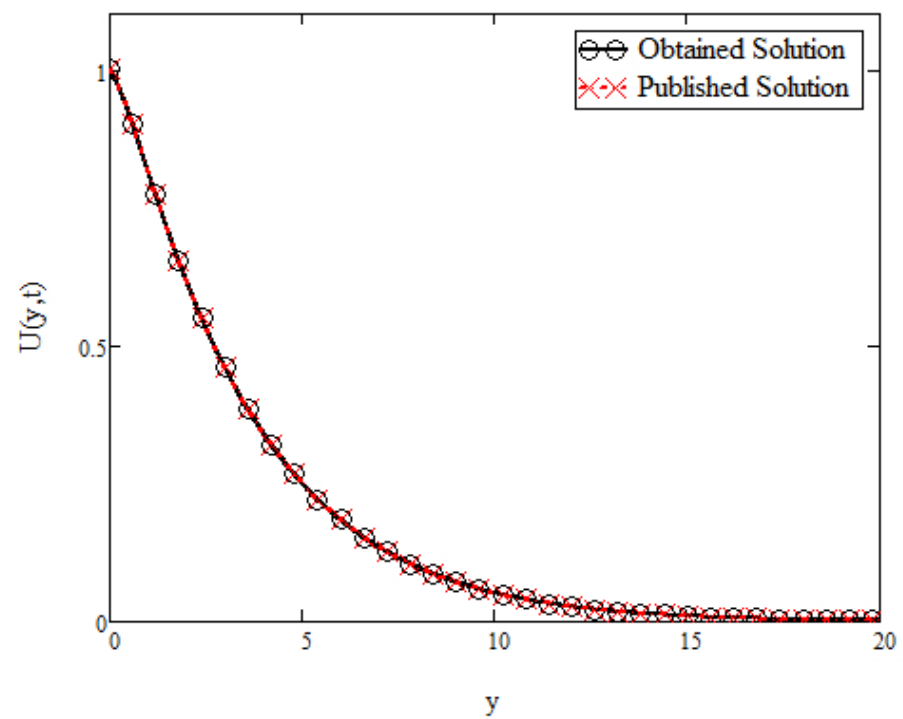


**Figure 5.** Comparison between published results from Ali et al. [35] and present results from Equation (20) on the velocity profile.
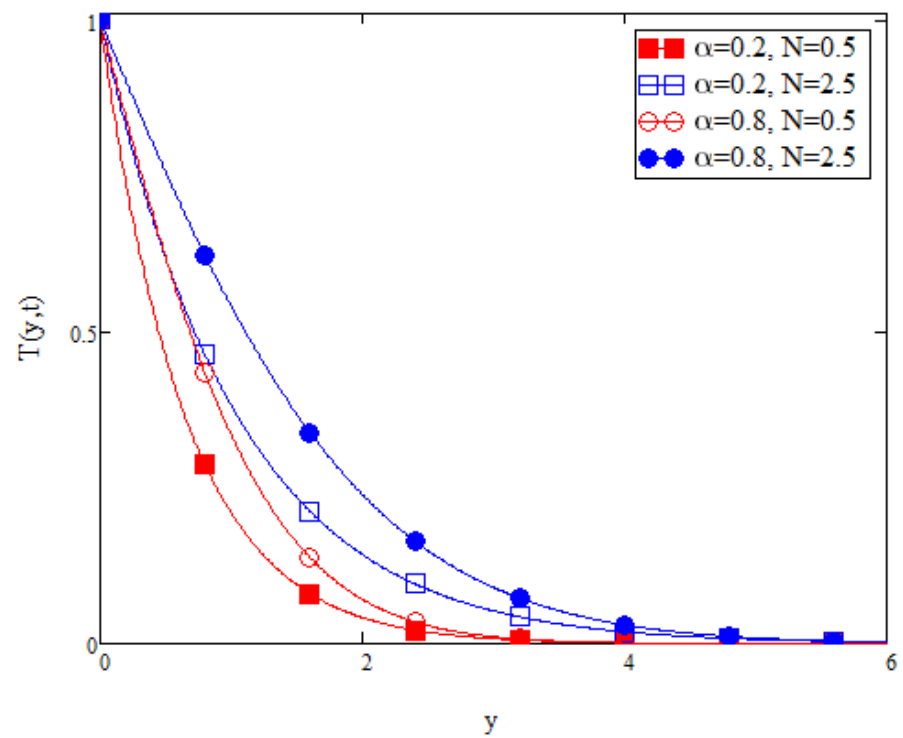
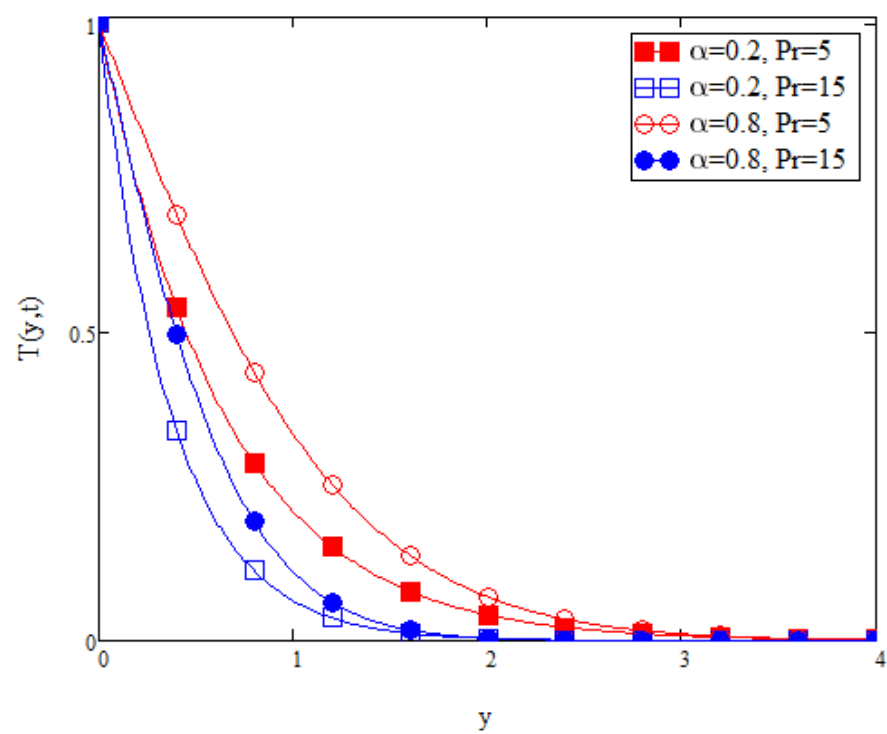**Figure 6.** Variation in energy profile due to variations in *N* and $\alpha$.



**Figure 7.** Variation in energy profile due to variations in *Pr* and $\alpha$.
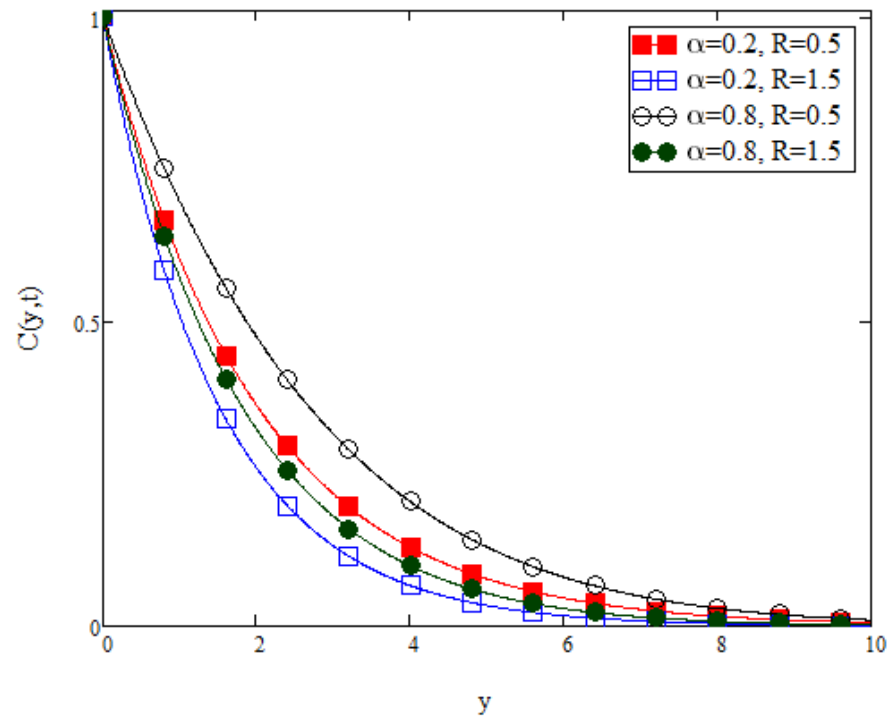
**Figure 8.** Variation in concentration profile due to variations in *R* and *α*.
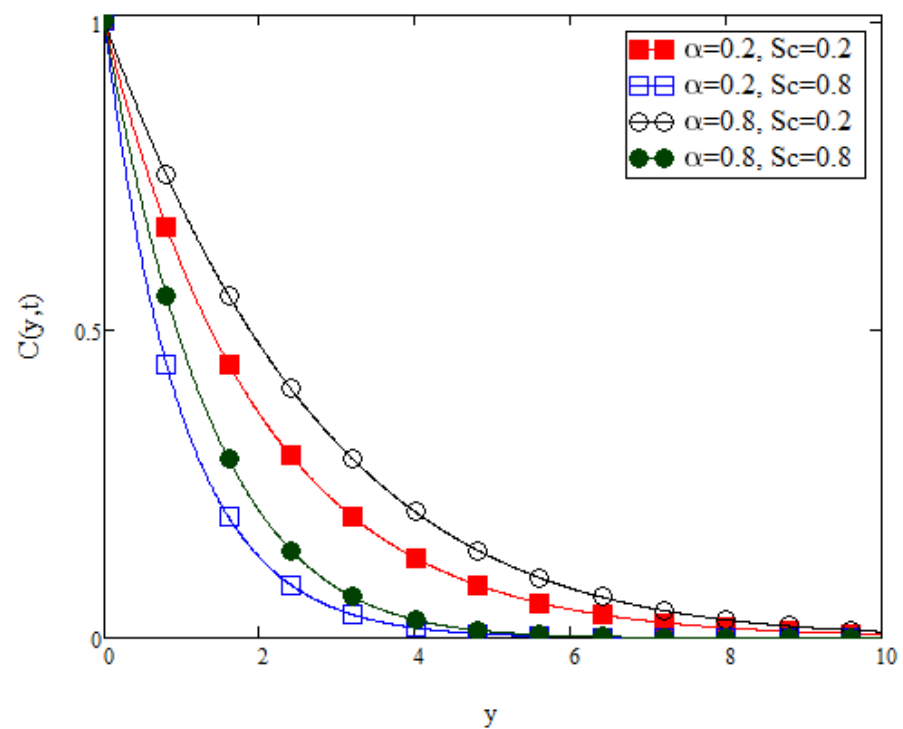


**Figure 9.** Variation in concentration profile due to variations in *Sc* and *α*.

Next, Figures 10–19 show velocity profiles with various values of *β*, *Gm*, *Gr*, *k'*, *M*, *N*, *Pr*, *R*, *Sc*, and *t*, respectively. Just like the temperature and concentration profiles, each figure from Figures 10–19 show variations in the fractional parameter, *α*, as well. To begin with, Figure 10 shows the velocity profile with variation in the Casson parameter, *β*. A Casson fluid is described as a shear thinning liquid with viscoplastic properties. If the shear rate is less than the yield stress, the fluid would behave as a Newtonian fluid. A fluctuation

in fluid behaviour is observed in Figure 10. Fluid velocity increases with an increase in $\beta$. After a certain point on the y-axis, as $\beta$ increases, viscosity of fluid would also increase and this resulted in the reduction of its velocity. From that point onward, fluid behaves as a non-Newtonian fluid instead of a Newtonian fluid. Figure 10 also shows that an increase in $\alpha$ resulted in an increase in the fluid velocity.



**Figure 10.** Variation in velocity profile due to variations in $\beta$ and $\alpha$.



**Figure 11.** Variation in velocity profile due to variations in *Gm* and $\alpha$.

**Figure 12.** Variation in velocity profile due to variations in *Gr* and $\alpha$.



**Figure 13.** Variation in velocity profile due to variations in *k'* and $\alpha$.
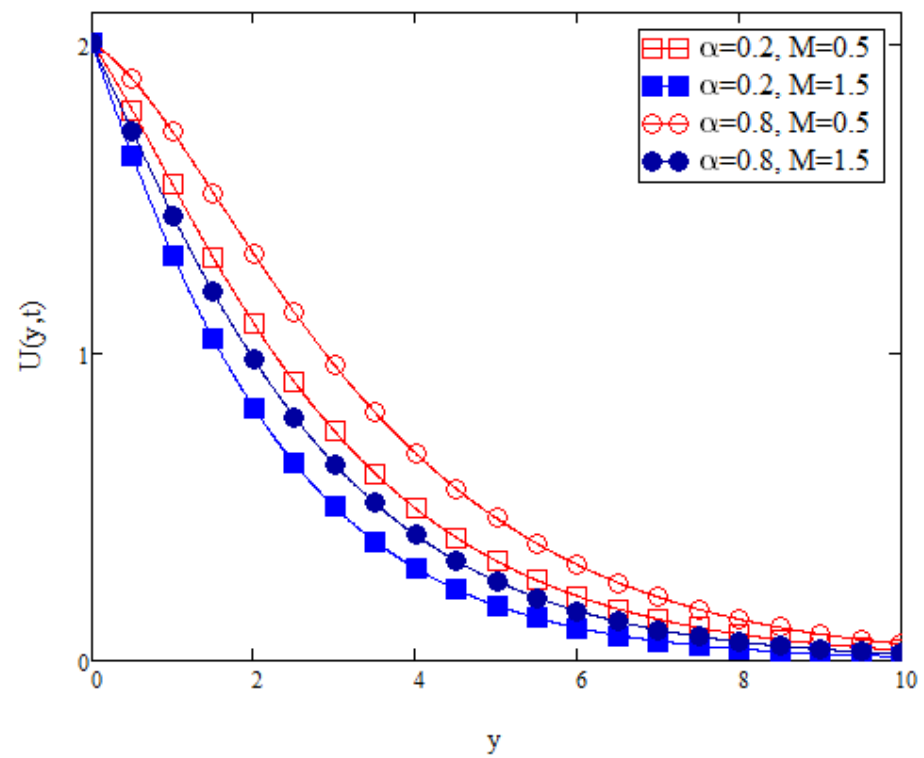
**Figure 14.** Variation in velocity profile due to variations in *M* and $\alpha$.
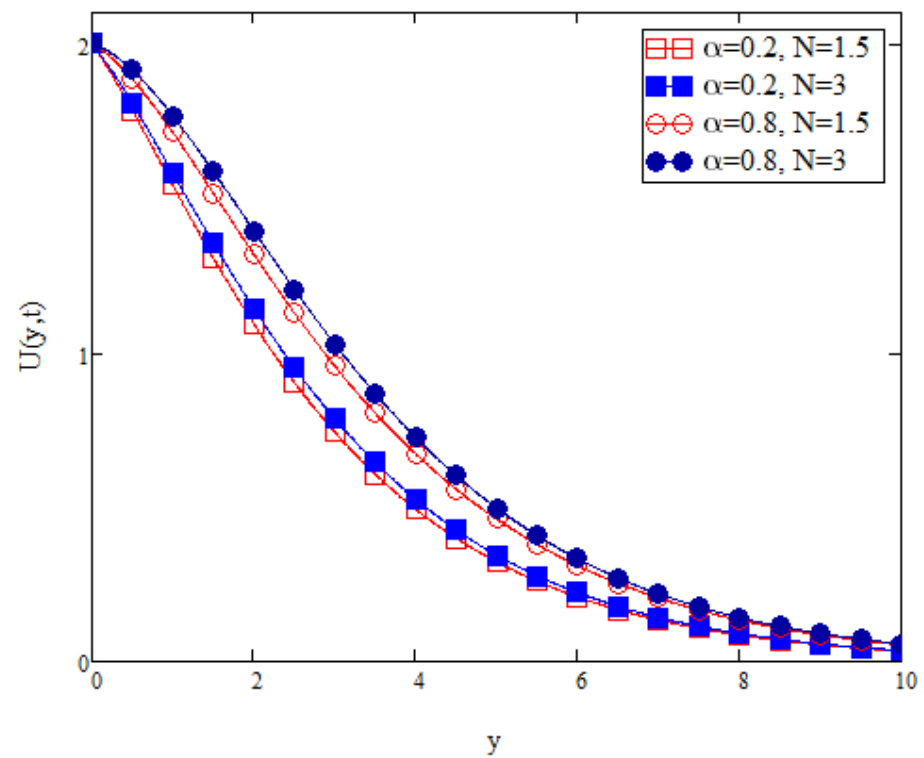
**Figure 15.** Variation in velocity profile due to variations in *N* and $\alpha$.
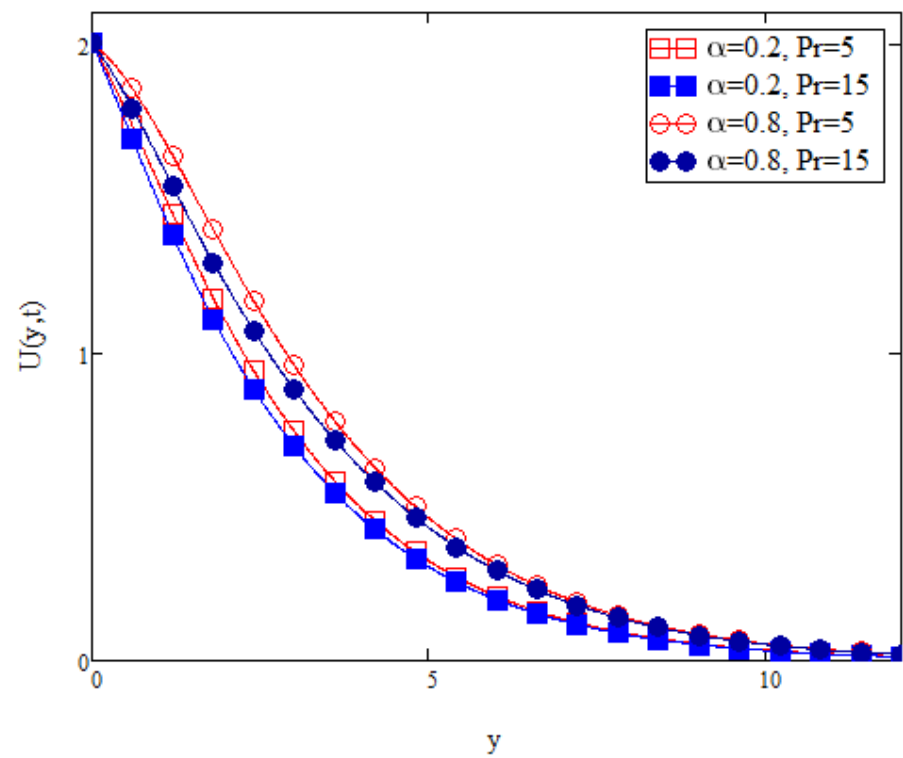
**Figure 16.** Variation in velocity profile due to variations in *Pr* and *α*.
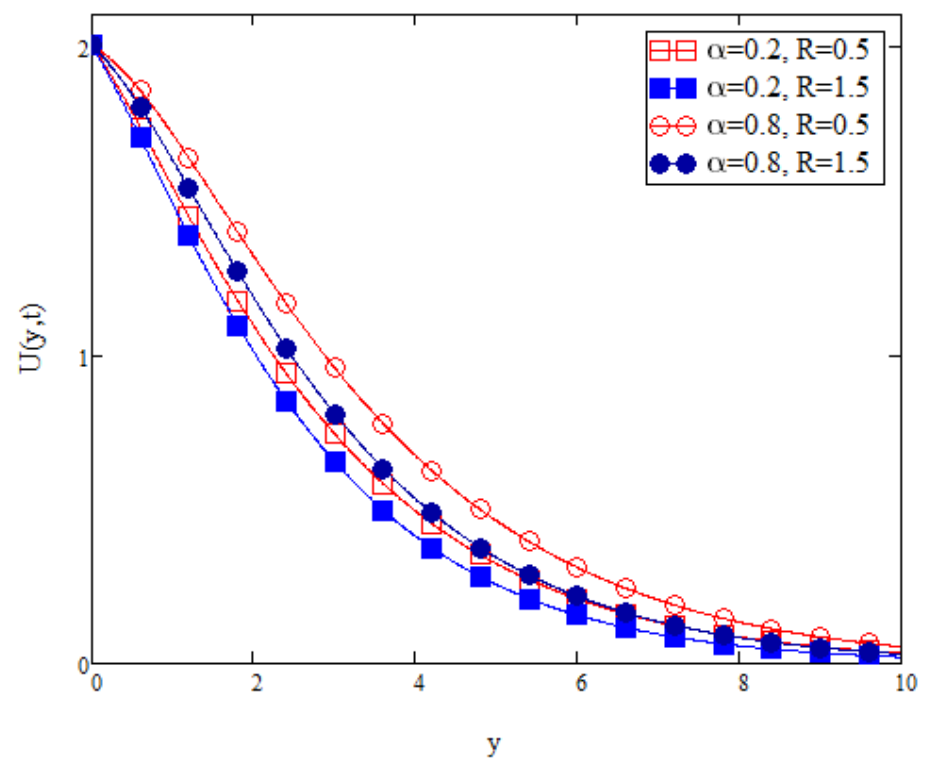


**Figure 17.** Variation in velocity profile due to variations in *R* and *α*.
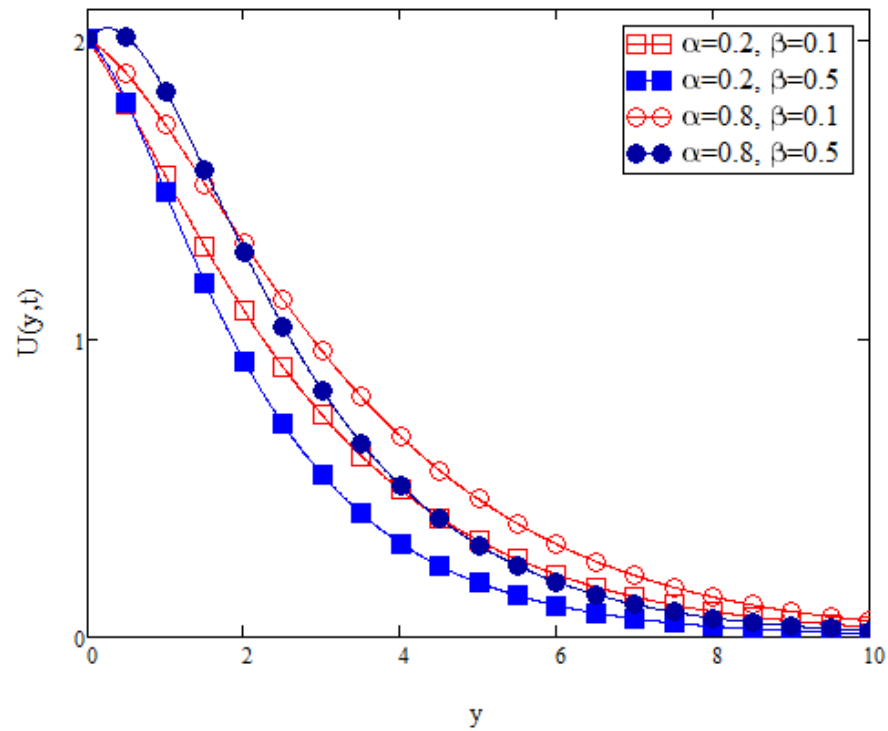
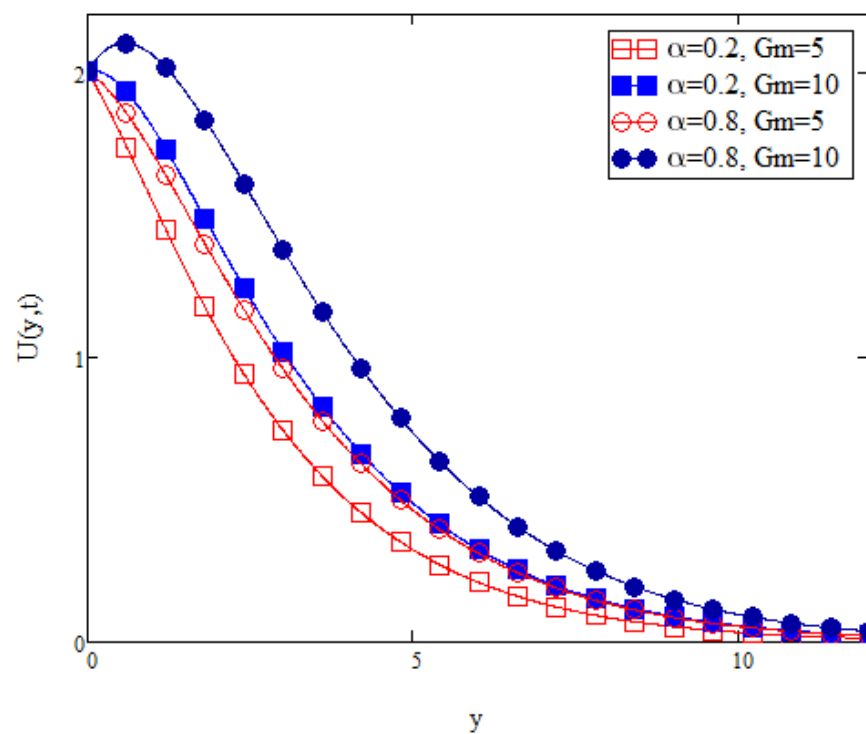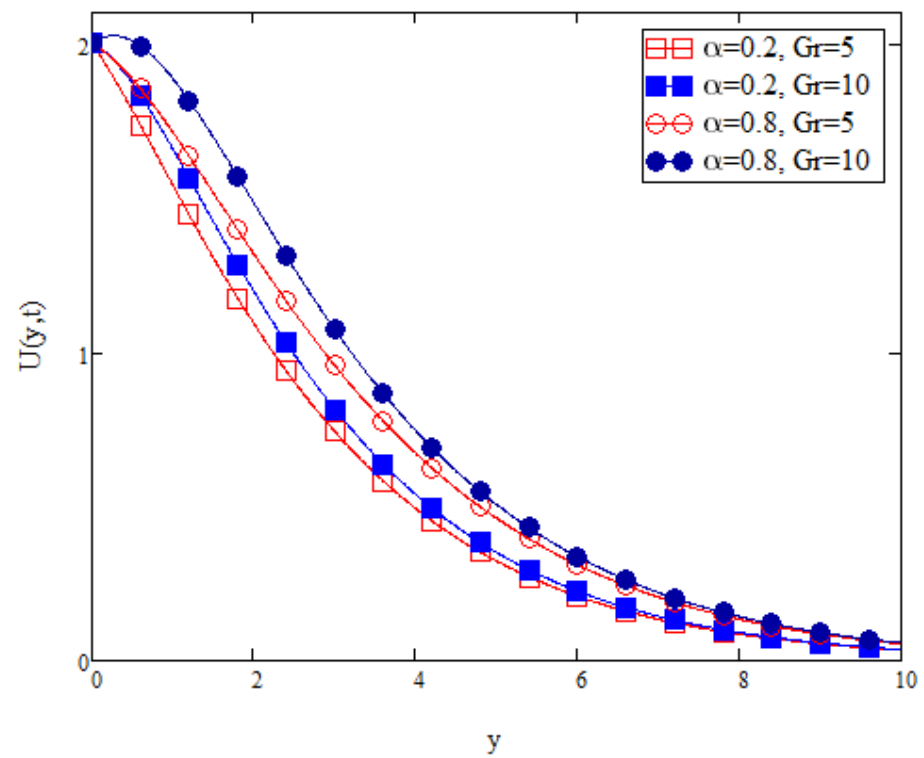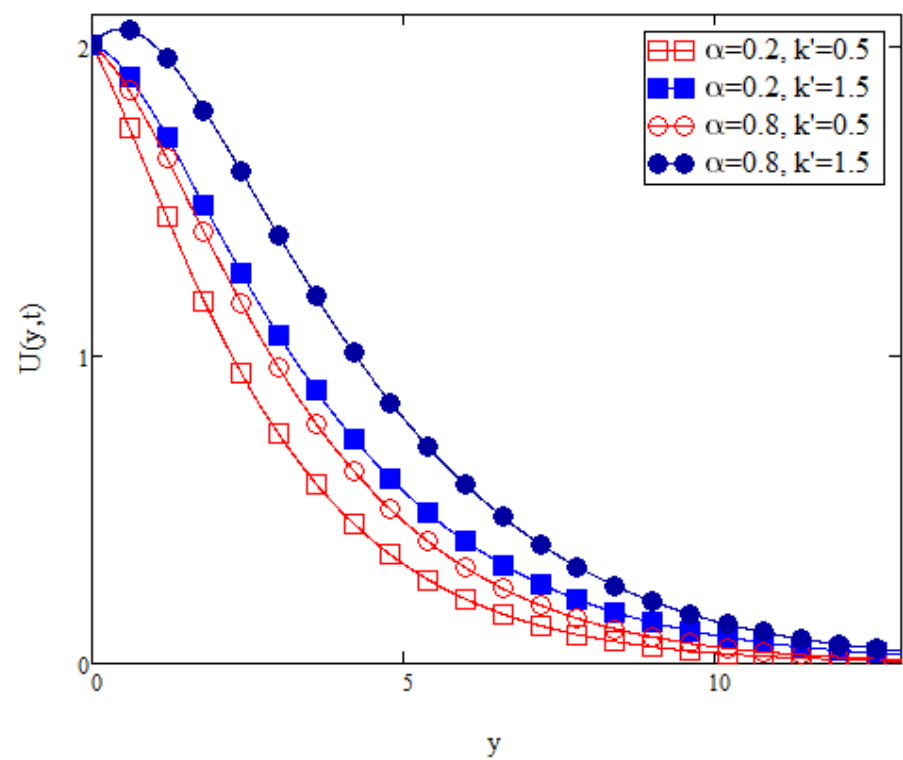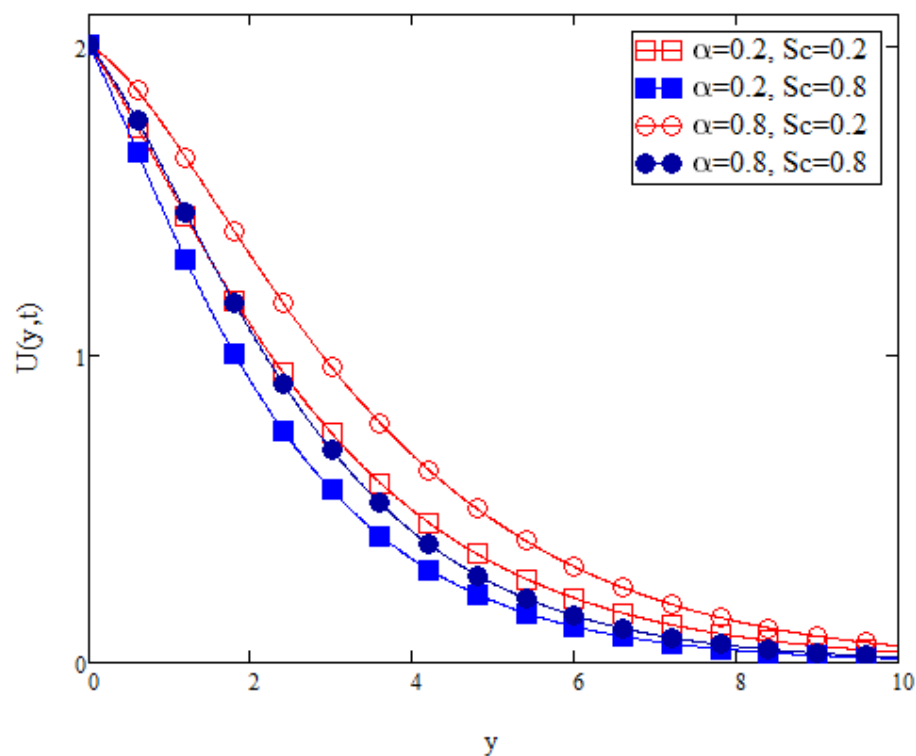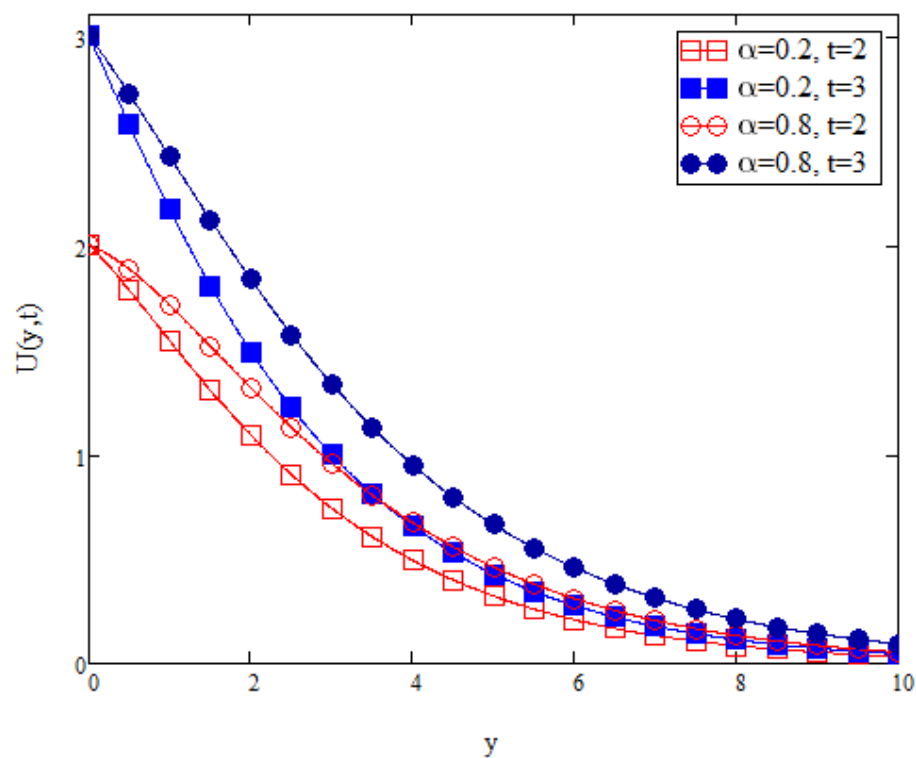**Figure 18.** Variation in velocity profile due to variations in *Sc* and *α*.



**Figure 19.** Variation in velocity profile due to variations in *t* and *α*.

Figure 11 displays the fluid velocity with variation in the mass Grashof number, *Gm*. A mass Grashof number is described as the ratio between the buoyancy force and the viscous hydrodynamic force. As the value of *Gm* increases, the buoyancy force on the fluid flow

increases and the viscous hydrodynamic force decreases. As the fluid flow considered in this study is flowing along a vertical plate, an increase in the buoyancy force would aid the velocity of fluid. Thus, as $Gm$ increases, the fluid velocity also increases. This behaviour is observed clearly in Figure 11. In addition in Figure 11, it is observed that if the fractional parameter, $\alpha$, is increased, velocity of fluid also increases.

Figure 12 depicts the velocity profile with variation in the thermal Grashof number, $Gr$. Similar to the mass Grashof number, a thermal Grashof number is the ratio between the buoyancy force and viscous hydrodynamic force. Unlike the mass Grashof number where the buoyancy force is dependent on the solutal volumetric expansion of the liquid, the buoyancy force of a thermal Grashof number is dependant on the thermal volumetric expansion of the liquid. Thus, increasing the $Gr$ consequently increases the buoyancy force. However, the increase in the buoyancy force is due to the thermal volumetric expansion, not the solutal volumetric expansion. As mentioned before, since the fluid flow considered is moving along the vertical plate, an increase in the buoyancy force ultimately increases the fluid velocity. It is also observed from Figure 12 that an increase in the fractional parameter, $\alpha$, resulted in an increase of the fluid velocity.

Figure 13 presents the impact of medium porosity, $k'$, on the velocity profile. As the value of $k'$ is increased, porosity of medium is also increased, providing more voids, or pores, thus limiting obstacles that produce friction against the fluid flow. Thus velocity of fluid increases with an increase in porous medium parameter $k'$. From Figure 13, it is observed that an increase in the fractional parameter $\alpha$, resulted in an increase in the fluid velocity.

Figure 14 shows the velocity profile with variation in the magnetohydrodynamic (MHD) parameter, $M$. Presence of MHD is usually indicated by presence of a magnetic field nearby the fluid flow. The induced magnetic field is possibly due to the presence of a magnetic material or even presence of an electrical current that induces magnetic fields. As the MHD parameter increases, the pulling force from the magnetic field also increases. This in turn hinders the fluid flow, thus decreasing the fluid velocity. Similarly, Figure 14 shows an increase in fluid velocity with an increase in fractional parameter $\alpha$.

Figure 15 displays the velocity profile with variation in thermal radiation effect, $N$. As mentioned, an increase in the thermal radiation ultimately increases the presence of heat in the fluid flow. This in turns increases the kinetic energy of the fluid and velocity of fluid increases. Thus, as observed in Figure 15, if the value of $N$ is increased, velocity of fluid also increases. In addition, in Figure 15, it is observed that an increase in fractional parameter $\alpha$ also increases the fluid velocity.

Figure 16 illustrates the fluid velocity profile with variation in the Prandtl value, $Pr$. As mentioned before, an increase in Pr, increases the momentum diffusivity and decreases the thermal diffusivity. Momentum diffusivity is directly related to an external pressure, the Shear stress, or both. Increasing the momentum diffusivity indicates that an external pressure is applied or the Shear stress is increased. This in turn hinders the fluid flow, decreasing its velocity. Thus, as observed in Figure 16, the velocity profile decreases when Pr is increased. From Figure 16, it is observed that fluid velocity increases with an increase in fractional parameter $\alpha$.

Figure 17 displays the fluid velocity profile with variation in the chemical reaction effect, $R$. As mentioned previously, the chemical reaction considered in this study is a destructive chemical reaction. An increase in $R$ indicates a more active destructive chemical reaction. Since a destructive chemical reaction creates a massive disturbance, fluid flow is indefinitely disrupted. Thus, when the value of $R$ is increased, the velocity decreases. Figure 17 also shows that the fluid velocity increases with an increase in fractional parameter $\alpha$.

Figure 18 depicts the fluid velocity profile with variation in Schmidt number, $Sc$. As mentioned before, the Schmidt number is defined as the ratio of the momentum diffusivity and the mass diffusivity. An increase in the value of $Sc$ indicates an increase in the momentum diffusivity. An increase in the momentum diffusivity is likely due to an external pressure applied onto the fluid or an increase in the shear stress or both. Either one

of these cases could interrupt the flow of fluid. Thus, as observed in Figure 18, an increase in the value of *Sc* decelerates the fluid flow. It also shows that an increase in the fractional parameter $\alpha$, increases the fluid velocity.

Figure 19 illustrates the fluid velocity profile with variation in time, *t*. In this study, it is considered that the fluid is flowing over a vertical uniformly accelerated plate. This in turn creates an initial condition, such as Equation (4), where initially the velocity of the fluid is at *At*. Through the process of non-dimensionalisation, the initial velocity is derived as Equation (10), where the velocity of fluid is initially at *t*. Thus, with an increase in *t*, the initial velocity of fluid increases as well, satisfying the boundary conditions. Figure 19 also shows that the fluid velocity increases with an increase in the fractional parameter $\alpha$.

Aforementioned, based on Figures 10–19, it is observed that the velocity profile increases with the increment of $\alpha$. To further investigate the impact of fractional derivatives on an MHD Casson fluid flowing over an accelerated plate, a comparison between the fractional derivative solution, from Equation (20) and a classical, non-fractional, derivative solution, from Equation (30), were conducted. Analysis of this comparison is displayed in Figure 20. It is shown that the non-fractional solution produces a velocity profile that is higher than the fractional solution. Observing the pattern of an increasing fractional parameter from Figures 10–19 as well as Figure 20, it can be suggested that higher values of fractional derivative parameter provide solutions that achieve steady state later compared to a lower values of the fractional parameter. Thus, it can be inferred that fractional parameters arising from fractional derivatives do have an impact on the velocity of a fluid. Although there is yet a geometrical application of fractional derivatives in the field of fluid flow, obtained solutions will be useful in validating experimental studies that will be carried out in the future. Figure 20 also illustrates analytical solutions for both velocity profiles, with and without fractional derivatives, that is plotted against their respective semi-analytical solutions to be validated. Henceforth, both solutions are valid since they fit perfectly with their corresponding semi-analytical solutions.
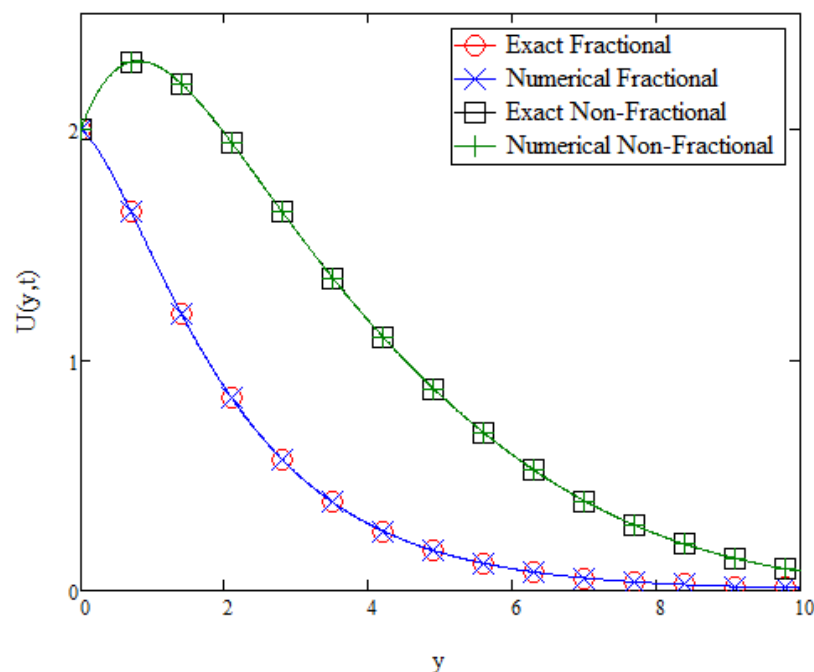


**Figure 20.** Comparison and numerical validations of solutions with fractional, from Equation (20), and non-fractional derivatives, from Equation (30), for the Casson fluid flow.

Tables 1–3 displays the Nusselt number, Sherwood number, and skin friction of the fluid flow with variations in the parametric values. From Table 1 it is observed that the Nusselt number increases with increment in Pr but decreases with increment in $\alpha$ and *N*. The Nusselt number is defined as the ratio between the convective heat transfer and

the conductive heat transfer. Increasing the Prandtl value resulted in the reduction of the thermal diffusion. This causes the conductive heat transfer in the fluid to be lowered and therefore increasing the Nusselt number value. This is the opposite when raising the thermal radiation value, $N$. Increasing the value of $N$ would ultimately increases the temperature of the fluid, thus increasing the conductive heat transfer and consequently reducing the Nusselt number value. From Table 2, it is observed that the Sherwood number increases as the values of $Sc$ and $R$ increases but decreases as $\alpha$ increases. The Sherwood number is described as the ratio between the convective mass transfer and the diffusivity of mass. Increasing the Schmidt value resulted in the reduction of the mass diffusivity, coherently increasing the Sherwood number. Similarly, increasing the chemical reaction rate, $R$, would cause an increase in the mass convection rate, thus increasing the Sherwood number. Table 3 shows that the skin friction increases with the increment of $Pr$, $Sc$, $R$, and $M$, but decreases with the increment of $\alpha$, $\beta$, $Gr$, $Gm$, $N$, and $k'$. The skin friction value is the result of frictional shear force exerted to the fluid parallel to the flow. A higher skin friction value is the result of a higher drag force created from the friction of the plate surface. According to Figures 10–19, higher values of $Pr$, $Sc$, $R$, and $M$ resulted in lower fluid velocity, while higher values of $\alpha$, $\beta$, $Gr$, $Gm$, $N$, and $k'$ resulted in a higher fluid velocity. This reflects excellently on the result of skin friction, where lower fluid velocities have higher skin friction and higher fluid velocities have lower skin friction.

**Table 1.** Nusselt number with various values of parameters.

| $\alpha$ | $Pr$ | $N$ | $Nu$ | Result |
|---|---|---|---|---|
| 0.2 | 5 | 0.5 | 1.532 | - |
| 0.8 | 5 | 0.5 | 0.802 | ↓ |
| 1.0 | 5 | 0.5 | −0.515 | ↓ |
| 0.2 | 15 | 0.5 | 2.653 | ↑ |
| 0.2 | 5 | 2.5 | 0.950 | ↓ |

**Table 2.** Sherwood number with various values of parameters.

| $\alpha$ | $Sc$ | $R$ | $Sh$ | Result |
|---|---|---|---|---|
| 0.2 | 0.2 | 0.5 | 0.505 | - |
| 0.8 | 0.2 | 0.5 | 0.349 | ↓ |
| 1.0 | 0.2 | 0.5 | −0.037 | ↓ |
| 0.2 | 0.8 | 0.5 | 1.010 | ↑ |
| 0.2 | 0.2 | 1.5 | 0.674 | ↑ |

**Table 3.** Skin friction with various values of parameters.

| $\alpha$ | $t$ | $\beta$ | $Pr$ | $Gr$ | $Gm$ | $Sc$ | $N$ | $R$ | $k'$ | $M$ | $\gamma$ | Result |
|---|---|---|---|---|---|---|---|---|---|---|---|---|
| 0.2 | 2 | 0.1 | 5.0 | 5.0 | 5.0 | 0.2 | 1.5 | 0.5 | 0.5 | 0.5 | 0.376 | - |
| 0.8 | 2 | 0.1 | 5.0 | 5.0 | 5.0 | 0.2 | 1.5 | 0.5 | 0.5 | 0.5 | 0.149 | ↓ |
| 1.0 | 2 | 0.1 | 5.0 | 5.0 | 5.0 | 0.2 | 1.5 | 0.5 | 0.5 | 0.5 | −0.847 | ↓ |
| 0.2 | 3 | 0.1 | 5.0 | 5.0 | 5.0 | 0.2 | 1.5 | 0.5 | 0.5 | 0.5 | 0.855 | ↑ |
| 0.2 | 2 | 0.5 | 5.0 | 5.0 | 5.0 | 0.2 | 1.5 | 0.5 | 0.5 | 0.5 | 0.208 | ↓ |
| 0.2 | 2 | 0.1 | 15.0 | 5.0 | 5.0 | 0.2 | 1.5 | 0.5 | 0.5 | 0.5 | 0.467 | ↑ |
| 0.2 | 2 | 0.1 | 5.0 | 10.0 | 5.0 | 0.2 | 1.5 | 0.5 | 0.5 | 0.5 | 0.107 | ↓ |
| 0.2 | 2 | 0.1 | 5.0 | 5.0 | 10.0 | 0.2 | 1.5 | 0.5 | 0.5 | 0.5 | −0.063 | ↓ |
| 0.2 | 2 | 0.1 | 5.0 | 5.0 | 5.0 | 0.8 | 1.5 | 0.5 | 0.5 | 0.5 | 0.521 | ↑ |
| 0.2 | 2 | 0.1 | 5.0 | 5.0 | 5.0 | 0.2 | 3.0 | 0.5 | 0.5 | 0.5 | 0.327 | ↓ |
| 0.2 | 2 | 0.1 | 5.0 | 5.0 | 5.0 | 0.2 | 1.5 | 1.5 | 0.5 | 0.5 | 0.437 | ↑ |
| 0.2 | 2 | 0.1 | 5.0 | 5.0 | 5.0 | 0.2 | 1.5 | 0.5 | 1.5 | 0.5 | 0.038 | ↓ |
| 0.2 | 2 | 0.1 | 5.0 | 5.0 | 5.0 | 0.2 | 1.5 | 0.5 | 0.5 | 1.5 | 0.749 | ↑ |

## 5. Conclusions

In this study, analytical fractional Casson fluid flow over an accelerated plate in porous medium with the presence of MHD, non-linear thermal radiation, and chemical reaction using Caputo-Fabrizio definition has been studied.

The velocity, temperature, and concentration profiles for the fluid flow were analysed graphically. The values of the Nusselt number, the Sherwood number, and the skin friction were numerically obtained and it is found that these numbers corresponds extremely well with the obtained results from the velocity, temperature, and concentration profiles. Through this study, it can be concluded that fractional derivatives do have an impact on the flow of an unsteady MHD Casson fluid over an accelerated plate with a porosity, thermal radiation, and chemical reaction effect.

**Author Contributions:** Conceptualisation, A.Q.M., M.S. and S.S.; methodology, R.R. and Y.J.L.; software, R.R.; validation, R.R., Y.J.L. and A.Q.M.; formal analysis, R.R.; investigation, R.R. and Y.J.L.; resources, R.R.; writing—original draft preparation, R.R.; writing—review and editing, R.R., Y.J.L., M.S. and A.Q.M.; visualisation, R.R.; supervision, A.Q.M., Y.J.L. and S.S.; project administration, S.S.; funding acquisition, S.S. All authors have read and agreed to the published version of the manuscript.

**Institutional Review Board Statement:** Not applicable.

**Informed Consent Statement:** Not applicable.

**Data Availability Statement:** Not applicable.

**Conflicts of Interest:** The authors declare no conflict of interest.

## Abbreviations

| | |
|---|---|
| AB | Atangana-Baleanu |
| CF | Caputo-Fabrizio |
| LES | Large Eddy Simulation |
| MHD | Magnetohydrodynamic |
| **Greek Symbols** | |
| $\alpha$ | Fractional derivative parameter |
| $\beta$ | Casson parameter |
| $\beta_0$ | Dimensionless Casson parameter |
| $\beta_C$ | Volumetric expansion (mol$^{-1}\cdot$ m$^3$) |
| $\beta_T$ | Thermal expansion (K$^{-1}$) |
| $\mu$ | Fluid dynamic viscosity (kg$\cdot$ m$^{-1}\cdot$ s$^{-1}$) |
| $\nu$ | Fluid kinematic viscosity (m$^2\cdot$ s$^{-1}$) |
| $\rho$ | Fluid density (kg$\cdot$ m$^{-3}$) |
| $\sigma$ | Electrical conductivity (S$\cdot$ m$^{-1}$) |
| $\sigma$ | Skin friction |
| $\sigma^*$ | Stefan-Boltzman constant (W$\cdot$ m$^{-2}\cdot$ K$^{-4}$) |
| **Symbols** | |
| $A$ | Plate acceleration (m$\cdot$ s$^{-2}$) |
| $a_{0\ldots14}$ | Dimensionless parametric constant |
| $B_0$ | Magnetic field (kg$\cdot$ s$^{-2}\cdot$ A$^{-1}$) |
| $b_{1\ldots4}$ | Dimensionless parametric constant |
| $C$ | Fluid concentration (mol$\cdot$ m$^{-3}$) |
| $C_\infty$ | Ambient concentration (mol$\cdot$ m$^{-3}$) |

| $C_P$ | Specific heat capacity ($J \cdot kg^{-1} \cdot K^{-1}$) |
|---|---|
| $C_W$ | Wall concentration ($mol \cdot m^{-3}$) |
| $D$ | Mass diffusion coefficient ($m^{-3}$) |
| $D_t^\alpha f$ | Caputo-Fabrizio fractional derivative |
| $g$ | Gravitational force ($m \cdot s^{-2}$) |
| $Gm$ | Mass Grashof number |
| $Gm_0$ | Dimensionless parametric constant |
| $Gr$ | Thermal Grashof number |
| $Gr_0$ | Dimensionless parametric constant |
| $k'$ | Dimensionless porosity parameter |
| $k$ | Porosity ($m^3$) |
| $k^*$ | Mean absorption coefficient ($m^{-1}$) |
| $k'_0$ | Dimensionless parametric constant |
| $k_1$ | Thermal conductivity ($W \cdot m^{-1} \cdot K^{-1}$) |
| $k_2$ | Chemical reaction ($mol \cdot m^{-3} \cdot s^{-1}$) |
| $M$ | Dimensionless magnetic parameter |
| $M_0$ | Dimensionless parametric constant |
| $N$ | Dimensionless thermal radiation parameter |
| $Nu$ | Nusselt number |
| $Pr$ | Prandtl number |
| $Pr_0$ | Dimensionless parametric constant |
| $q$ | Frequency ($s^{-1}$) |
| $q_r$ | Thermal radiation ($W \cdot m^{-2}$) |
| $R$ | Dimensionless chemical reaction parameter |
| $R_0$ | Dimensionless parametric constant |
| $Sc$ | Schmidt number |
| $Sh$ | Sherwood number |
| $T$ | Fluid temperature (K) |
| $t$ | Time (s) |
| $T_\infty$ | Ambient temperature (K) |
| $T_W$ | Wall temperature (K) |
| $U$ | Fluid velocity ($m \cdot s^{-1}$) |
| $x$ | x-coordinate |
| $y$ | y-coordinate |

## References

1. Pramanik, S. Casson fluid flow and heat transfer past an exponentially porous stretching surface in presence of thermal radiation. *Ain Shams Eng. J.* **2014**, *5*, 205–212. [CrossRef]
2. Artemov, E.S.; Baranovskii, M.A. Global Existence Results for Oldroyd Fluids with Wall Slip. *Acta Appl. Math.* **2017**, *147*, 197–210. [CrossRef]
3. Sheikh, M.; Abbas, Z. Homogeneous–Heterogeneous reactions in stagnation point flow of Casson fluid due to a stretching/shrinking sheet with uniform suction and slip effects. *Ain Shams Eng. J.* **2017**, *8*, 467–474. [CrossRef]
4. Casson, N. A flow equation for pigment-oil suspensions of the printing ink type. In *Rheology of Disperse Systems*; Pergamon: Oxford, UK, 1959.
5. Liu, C.; Zheng, L.; Lin, P.; Pan, M.; Liu, F. Anomalous diffusion in rotating Casson fluid through a porous medium. *Phys. A Stat. Mech. Appl.* **2019**, *528*, 121431. [CrossRef]
6. Maiti, S.; Shaw, S.; Shit, G.C. Caputo–Fabrizio fractional order model on MHD blood flow with heat and mass transfer through a porous vessel in the presence of thermal radiation. *Phys. A Stat. Mech. Appl.* **2020**, *540*, 123149. [CrossRef]
7. Frigaard, I. Simple yield stress fluids. *Curr. Opin. Colloid Interface Sci.* **2019**, *43*, 80–93. [CrossRef]
8. Gbadeyan, J.A.; Titiloye, E.O.; Adeosun, A.T. Effect of variable thermal conductivity and viscosity on Casson nanofluid flow with convective heating and velocity slip. *Heliyon* **2020**, *6*, e03076. [CrossRef]
9. Hussanan, A.; Salleh, M.Z.; Tahar, R.M.; Khan, I. Unsteady boundary layer flow and heat transfer of a Casson fluid past an oscillating vertical plate with Newtonian heating. *PLoS ONE* **2014**, *9*, e108763. [CrossRef]
10. Hussanan, A.; Salleh, M.Z.; Khan, I.; Tahar, R.M. Heat transfer in magnetohydrodynamic flow of a casson fluid with porous medium and newtonian heating. *J. Nanofluids* **2017**, *6*, 784–793. [CrossRef]
11. Khalid, A.; Khan, I.; Shafie, S. Exact solutions for unsteady free convection flow of Casson fluid over an oscillating vertical plate with constant walal temperature. In *Abstract and Applied Analysis*; Hindawi: London, UK, 2015; Volume 2015.
12. Khalid, A.; Khan, I.; Khan, A.; Shafie, S. Unsteady MHD free convection flow of Casson fluid past over an oscillating vertical plate embedded in a porous medium. *Eng. Sci. Technol. Int. J.* **2015**, *18*, 309–317. [CrossRef]

13. Kataria, H.R.; Patel, H.R. Radiation and chemical reaction effects on MHD Casson fluid flow past an oscillating vertical plate embedded in porous medium. *Alex. Eng. J.* **2016**, *55*, 583–595. [CrossRef]

14. Khan, D.; Khan, A.; Khan, I.; Ali, F.; ul Karim, F.; Tlili, I. Effects of Relative Magnetic Field, Chemical Reaction, Heat Generation and Newtonian Heating on Convection Flow of Casson Fluid over a Moving Vertical Plate Embedded in a Porous Medium. *Sci. Rep.* **2019**, *9*, 1–18. [CrossRef]

15. Kataria, H.R.; Patel, H.R. Effects of chemical reaction and heat generation/absorption on magnetohydrodynamic (MHD) Casson fluid flow over an exponentially accelerated vertical plate embedded in porous medium with ramped wall temperature and ramped surface concentration. *Propuls. Power Res.* **2019**, *8*, 35–46. [CrossRef]

16. Naqvi, S.M.R.S.; Muhammad, T.; Asma, M. Hydromagnetic flow of Casson nanofluid over a porous stretching cylinder with Newtonian heat and mass conditions. *Phys. A Stat. Mech. Appl.* **2020**, *550*, 123988. [CrossRef]

17. Ramalingeswara Rao, S.; Vidyasagar, G.; Deekshitulu, G. Unsteady MHD free convection Casson fluid flow past an exponentially accelerated infinite vertical porous plate through porous medium in the presence of radiation absorption with heat generation/absorption. *Mater. Today. Proc.* **2020**, *42*, 1608–1616. [CrossRef]

18. Khan, I.; Shah, N.A.; Vieru, D. Unsteady flow of generalized Casson fluid with fractional derivative due to an infinite plate. *Eur. Phys. J. Plus* **2016**, *131*, 181. [CrossRef]

19. Leibniz, G.W. Letter from Hanover, Germany, September 30, 1695, to GA L'Hospital. *JLeibnizen Math. Schr.* **1849**, *2*, 1849.

20. Ross, B. A brief history and exposition of the fundamental theory of fractional calculus. In *Fractional Calculus and Its Applications*; Springer: Berlin/Heidelberg, Germany, 1975; pp. 1–36. [CrossRef]

21. Malinowska, A.B.; Torres, D.F. Fractional calculus of variations for a combined Caputo derivative. *Fract. Calc. Appl. Anal.* **2011**, *14*, 523–537. [CrossRef]

22. Loverro, A. *Fractional Calculus: History, Definitions and Applications for the Engineer*; Rapport technique; Univeristy of Notre Dame, Department of Aerospace and Mechanical Engineering: Notre Dame, IN, USA, 2004; pp. 1–28.

23. Atangana, A.; Baleanu, D. New fractional derivatives with nonlocal and non-singular kernel: Theory and application to heat transfer model. *Therm. Sci.* **2016**, *20*, 763–769. [CrossRef]

24. Cao, D.; Lopes, A.M.; Machado, J.A.T. Time-fractional dependence of the shear force in some beam type problems with negative Young modulus. *Appl. Math. Model.* **2020**, *80*, 668–682. [CrossRef]

25. Gómez-aguilar, J.F.; Yépez-martínez, H.; Escobar-jiménez, R.F. Analytical and numerical solutions of electrical circuits described by fractional derivatives. *Appl. Math. Model.* **2016**, *40*, 9079–9094. [CrossRef]

26. Atangana, A.; Baleanu, D. Caputo-Fabrizio Derivative Applied to Groundwater Flow within Confined Aquifer. *J. Eng. Mech.* **2017**, *143*, D4016005. [CrossRef]

27. Atangana, A. *Fractional Operators with Constant and Variable Order with Application to Geo-Hydrology*; Academic Press: London, UK, 2017.

28. Yuan, B.; Zhang, Q. Global well-posedness of the d-D Oldroyd-B type models with fractional Laplacian dissipation. *Comput. Math. Appl.* **2019**, *77*, 1933–1944. [CrossRef]

29. Saad, K.M.; Baleanu, D.; Atangana, A. New fractional derivatives applied to the Korteweg—De Vries and Korteweg—De Vries—Burger' s equations. *Comput. Appl. Math.* **2018**, *37*, 5203–5216. [CrossRef]

30. Saad, K.M.; Atangana, A.; Baleanu, D.; Saad, K.M.; Atangana, A.; Baleanu, D. New fractional derivatives with non-singular kernel applied to the Burgers equation New fractional derivatives with non-singular kernel applied to the Burgers equation. *Chaos* **2018**, *28*, 063109. [CrossRef] [PubMed]

31. Egolf, P.W.; Hutter, K. *Nonlinear, Nonlocal and Fractional Turbulence*; Springer International Publishing: Cham, Switzerland, 2019.

32. Samiee, M.; Akhavan-Safaei, A.; Zayernouri, M. Tempered fractional LES modeling. *J. Fluid Mech.* **2021**, *932*, A4-1–A4-32. [CrossRef]

33. Seyedi, S.H.; Zayernouri, M. A Data-Driven Dynamic Nonlocal LES Model for Turbulent Flows. *arXiv* **2021**, arXiv:2111.10936.

34. Atangana, A.; Baleanu, D. Numerical Solution of a Kind of Fractional Parabolic Equations via Two Difference Schemes. *Abstract Appl. Anal.* **2013**, *2013*, 828764. [CrossRef]

35. Ali, F.; Sheikh, N.A.; Khan, I.; Saqib, M. Solutions with Wright Function for Time Fractional Free Convection Flow of Casson Fluid. *Arab. J. Sci. Eng.* **2017**, *42*, 2565–2572. [CrossRef]

36. Khan, I.; Saqib, M.; Ali, F. Application of time-fractional derivatives with non-singular kernel to the generalized convective flow of Casson fluid in a microchannel with constant walls temperature. *Eur. Phys. J. Spec. Top.* **2017**, *226*, 3791–3802. [CrossRef]

37. Sheikh, N.A.; Ali, F.; Saqib, M.; Khan, I.; Jan, S.A.A. A comparative study of Atangana-Baleanu and Caputo-Fabrizio fractional derivatives to the convective flow of a generalized Casson fluid. *Eur. Phys. J. Plus* **2017**, *132*. [CrossRef]

38. Sheikh, N.A.; Ali, F.; Saqib, M.; Khan, I.; Jan, S.A.A.; Alshomrani, A.S.; Alghamdi, M.S. Comparison and analysis of the Atangana–Baleanu and Caputo–Fabrizio fractional derivatives for generalized Casson fluid model with heat generation and chemical reaction. *Results Phys.* **2017**, *7*, 789–800. [CrossRef]

39. Qushairi, A.; Khan, I.; Yeou, L.; Shafie, S.; Mat, Z. Heat transfer on rotating second grade fluid through an accelerated plate. *Malays. J. Fundam. Appl. Sci.* **2017**, *13*, 218–222.

40. Khan, I. New idea of Atangana and Baleanu fractional derivatives to human blood flow in nanofluids. *Chaos Interdiscip. J. Nonlinear Sci.* **2019**, *29*, 13121. [CrossRef]

41. Pantokratoras, A. Natural convection along a vertical isothermal plate with linear and non-linear Rosseland thermal radiation. *Int. J. Therm. Sci.* **2014**, *84*, 151–157. [CrossRef]

42. Magyari, E.; Pantokratoras, A. Note on the effect of thermal radiation in the linearized Rosseland approximation on the heat transfer characteristics of various boundary layer flows. *Int. Commun. Heat Mass Transf.* **2011**, *38*, 554–556. [CrossRef]

43. Abro, K.A.; Gómez-Aguilar, J.F. A comparison of heat and mass transfer on a Walter's-B fluid via Caputo-Fabrizio versus Atangana-Baleanu fractional derivatives using the Fox-H function. *Eur. Phys. J. Plus* **2019**, *134*. [CrossRef]

44. Atangana, A. On the new fractional derivative and application to nonlinear Fisher's reaction-diffusion equation. *Appl. Math. Comput.* **2016**, *273*, 948–956. [CrossRef]

45. Jamil, D.F.; Uddin, S.; Kamardan, M.G.; Roslan, R. The effects of magnetic blood flow in an inclined cylindrical tube using caputo-fabrizio fractional derivatives. *CFD Lett.* **2020**, *12*, 111–122.